



HAL
open science

Experimental analysis of Delaunay flip algorithms on genus two hyperbolic surfaces

Vincent Despré, Loïc Dubois, Benedikt Kolbe, Monique Teillaud

► **To cite this version:**

Vincent Despré, Loïc Dubois, Benedikt Kolbe, Monique Teillaud. Experimental analysis of Delaunay flip algorithms on genus two hyperbolic surfaces. 2022. hal-03462834v2

HAL Id: hal-03462834

<https://inria.hal.science/hal-03462834v2>

Preprint submitted on 11 May 2022

HAL is a multi-disciplinary open access archive for the deposit and dissemination of scientific research documents, whether they are published or not. The documents may come from teaching and research institutions in France or abroad, or from public or private research centers.

L'archive ouverte pluridisciplinaire **HAL**, est destinée au dépôt et à la diffusion de documents scientifiques de niveau recherche, publiés ou non, émanant des établissements d'enseignement et de recherche français ou étrangers, des laboratoires publics ou privés.

Experimental analysis of Delaunay flip algorithms on genus two hyperbolic surfaces

Vincent Despré¹, Loïc Dubois², Benedikt Kolbe³, and Monique Teillaud⁴

¹Université de Lorraine, CNRS, Inria, LORIA, F-54000 Nancy, France
vincent.despre@loria.fr

²LIGM, CNRS, Université Gustave Eiffel, F-77454 Marne-la-Vallée, France *
loic.dubois@ens-lyon.fr

³Hausdorff Center for Mathematics, University of Bonn, Germany[†]
benedikt.kolbe@physik.hu-berlin.de

<https://hyperbolictilings.wordpress.com/>

⁴Université de Lorraine, CNRS, Inria, LORIA, F-54000 Nancy, France
monique.teillaud@inria.fr

<https://members.loria.fr/Monique.Teillaud>

May 11, 2022

Abstract

Guided by insights on the mapping class group of a surface, we give experimental evidence that the upper bound recently proven on the diameter of the flip graph of a closed oriented hyperbolic surface by Despré, Schlenker, and Teillaud (SoCG'20) is largely overestimated. To this aim, we develop an experimental framework for the storage of triangulations. We show that the computations with algebraic numbers can be overcome by proving a density result on rationally described genus two surfaces, and we propose ways to generate surfaces that are meaningful for the experiments.

Acknowledgements The authors want to thank Vincent Delecroix, Matthijs Ebbens, Hugo Parlier, Jean-Marc Schlenker, and Gert Vegter for helpful discussions over many years.

Source code available at <https://members.loria.fr/Monique.Teillaud/Exp-hyperb-flips/>.

Funding This work was partially supported by grant ANR-17-CE40-0033 of the French National Research Agency ANR (project SoS) <https://SoS.loria.fr/>.

*This work was done while this author was working at Université de Lorraine, CNRS, Inria, LORIA, F-54000 Nancy

[†]This work was done while this author was working at Université de Lorraine, CNRS, Inria, LORIA, F-54000 Nancy

Contents

- 1 Introduction** **1**

- 2 Background** **2**
 - 2.1 Hyperbolic surfaces 2
 - 2.2 Triangulations and flips on hyperbolic surfaces 2
 - 2.3 Mapping class group 2
 - 2.4 Admissible symmetric octagons 3

- 3 Representation of triangulations** **4**
 - 3.1 Data structure 4
 - 3.2 Flipping an edge 5

- 4 Solving arithmetic issues** **5**
 - 4.1 Issues when using algebraic numbers 5
 - 4.2 Density of the rationally described surfaces 6

- 5 The generation of the input for the experiments** **7**
 - 5.1 The twists of admissible loosely-symmetric octagons 8
 - 5.2 The generation of triangulations 8

- 6 Comparison of flip strategies** **10**

- 7 Exploring the relationship between number of flips and diameter** **13**
 - 7.1 Rationale for the experiments 13
 - 7.2 Exploring with power sequences 15
 - 7.3 Exploring with random sequences 15
 - 7.4 Interpretation of the results 16

- A Cross-ratios and Delaunay flips** **18**

- B Details for the representation of triangulations (Section 3)** **19**
 - B.1 On combinatorial maps and the anchor (Section 3.1) 19
 - B.2 Flipping edges (Section 3.2) 20

- C Details for solving arithmetic issues (Section 4)** **22**
 - C.1 Experiment on algebraic numbers (Section 4.1) 22
 - C.2 Approximation algorithm (Section 4.2) 22

- D Details for the generation of input (Section 5)** **24**
 - D.1 Generating an initial rational 4-tuple (step 1) 24
 - D.2 Generating points in an admissible symmetric octagon (step 2) 25
 - D.3 Constructing the data structure (step 4) 25

- E Computation of the approximation of the diameter (Section 7)** **26**

1 Introduction

It was recently proven that the geometric flip graph of a closed oriented hyperbolic surface is connected [7]. A Delaunay flip algorithm can thus transform any input geometric triangulation T , i.e., a triangulation whose edges are embedded as geodesic segments only intersecting at common endpoints, into a Delaunay triangulation. This is particularly useful in practice as a crucial preprocessing step to computing Delaunay triangulations on a surface: it transforms a “bad” representation of a surface, e.g., by a very elongated fundamental domain, to a “nice” representation by a Delaunay triangulation with only one vertex.

An upper-bound on the number of flips was proven [7, Theorem 19]: $C_h \cdot \Delta(T)^{6g-4} \cdot n^2$, where C_h is a constant, $\Delta(T)$ is the diameter of T , g is the genus of the surface, and n is the number of vertices. The diameter $\Delta(T)$ is the smallest diameter of a fundamental domain that is the union of lifts of the triangles of T in \mathbb{H} (note that this is not the diameter of the surface, which is independent of the representation). Computing it algorithmically seems difficult, however for a triangulation with only one vertex (thus with $4g - 2$ triangles) some bounds are easily derived: $L_T \leq \Delta(T) \leq \Delta(F) \leq L_T \cdot (4g - 2)$, where L_T denotes the maximal length of an edge of T and $F \subset \mathbb{H}$ is any fundamental domain made of lifts of the triangles of T . From these bounds we see that $\Delta(T)$ cannot differ too much from the diameter of any such F : in the case of a genus two surface they only differ by a factor of at most six. In the experiments, we will thus use the domain that naturally appears.

In this paper, we experimentally study the dependence of the number of flips on $\Delta(T)$ (Section 7), for surfaces of genus two. We suspect that the factor $\Delta(T)^{6g-4}$ is largely overestimated. It is derived from the number of paths of bounded length on a surface. Intuitively, for a length bounded by L , it roughly amounts to the volume of the ball of diameter L , so, it is exponential in L ; if only simple paths are considered, this number reduces to L^{6g-4} [7], but there is no reason why the flip algorithm would use all the simple paths shorter than L instead of going straight. More formally, our expectation on the dependence in $\Delta(T)$ is based on insights on the structure of the mapping class group (Section 2.3).

To perform experiments, we set up a framework consisting of various tools. In Section 3, we present a data structure for triangulations of surfaces, which supports flips; it relies on the representation of genus two surfaces by octagons in \mathbb{H} (Section 2.4). Not surprisingly, arithmetic issues quickly arise, as algebraic numbers are involved in the description of the octagons (Section 4.1). We overcome them by proving a density result on rationally described octagons (Section 4.2), which allows us to restrict to rational numbers in our experiments.

The generation of input surfaces and triangulations is far from trivial; it is a non-negligible part of our work (Section 5). We obtain surfaces with a large diameter by twisting the above-mentioned octagons (Section 5.1).

In Section 6, we run experiments comparing strategies on the sequence of edge flips, and conclude that the naive strategy is close to being the best one in practice. We adhere to it for our main experiments that study the dependence of the number of flips on $\Delta(T)$.

The way we conduct these experiments in Section 7 is inspired by previous work by Mark Bell [2] who studied flips in a topological setting. We focus on triangulations having only one vertex, both because the dependence on the number of vertices is easily seen, and because inserting a lot of points would rather be done by Bowyer’s incremental algorithm [13, 6], inspired from previous work in the flat case [17]. Quite surprisingly, in practice, we observe a behavior that is only expected asymptotically.

2 Background

2.1 Hyperbolic surfaces

All the surfaces considered in this paper are closed (connected, compact and without boundary), oriented, and hyperbolic. Consider such a hyperbolic surface \mathcal{S} of genus $g \geq 2$ and the underlying topological surface S_g . Given a hyperbolic structure h on \mathcal{S} , associated to a metric of constant curvature -1 , the surface $\mathcal{S} = (S_g, h)$ is isometric to the quotient \mathbb{H}/G , where \mathbb{H} is the hyperbolic plane and G is a (non-Abelian) discrete subgroup of the isometry group of \mathbb{H} isomorphic to the fundamental group $\pi_1(S_g)$.

The universal cover of \mathcal{S} is isometric to \mathbb{H} equipped with a projection $\rho : \mathbb{H} \rightarrow \mathcal{S}$ that is a local isometry. The group G acts on \mathbb{H} , so that for any $p \in \mathcal{S}$, $\rho^{-1}(p)$ is an orbit under the action of G . A lift \tilde{p} of a point $p \in \mathcal{S}$ is one of the elements of the orbit $\rho^{-1}(p)$.

We use the Poincaré disk model of \mathbb{H} , in which \mathbb{H} is represented as the open unit disk \mathbb{D} of the complex plane \mathbb{C} . Every orientation preserving isometry $f : \mathbb{D} \rightarrow \mathbb{D}$ can be represented by a matrix $\begin{pmatrix} a & b \\ c & d \end{pmatrix} \in \mathbb{C}^{2 \times 2}$ such that $f(z) = \frac{az + b}{cz + d}$ for any $z \in \mathbb{D}$. Observe that the matrix is not unique. In addition some matrices do not represent an isometry. Given two orientation preserving isometries f and g respectively represented by matrices A and B , the product $A \cdot B$ represents $f \circ g$.

2.2 Triangulations and flips on hyperbolic surfaces

A topological triangulation of a hyperbolic surface \mathcal{S} is any embedding of an undirected graph with a finite number of vertices onto \mathcal{S} such that each resulting face is homeomorphic to an open disk and is bounded by exactly three distinct edge-embeddings. Observe that this graph may have loops or multiple edges, and recall that the terms *embedding* and *embedded* subsume that edges only intersect at common vertices. A *geometric triangulation* is a topological triangulation of \mathcal{S} whose edges are embedded as geodesic segments [7]. All triangulations considered in this paper are geometric, so we just use the term *triangulation*. For any triangulation T of \mathcal{S} , the lift \tilde{T} of T is the (infinite) triangulation of \mathbb{H} whose vertices and edges are the lifts of the vertices and the edges of T . A *Delaunay triangulation* T of \mathcal{S} is a triangulation whose lift \tilde{T} is a Delaunay triangulation in \mathbb{H} . In other words, for each face t of T and any of its lifts \tilde{t} , the open disk in \mathbb{H} circumscribing \tilde{t} does not contain any vertex of \tilde{T} . Recall that circles in the Poincaré disk model correspond to circles in the complex plane.

Lifting an edge e of T to some \tilde{e} , together with the two triangles incident to \tilde{e} in the lifted triangulation \tilde{T} , we say that e is *Delaunay-flippable* if the open disks of these two triangles contain the fourth vertex of the quadrilateral formed by the two triangles. In this case, the geodesic segment \tilde{e}' that is the other diagonal of the quadrilateral is contained in it. The *Delaunay flip* of e in T consists in replacing \tilde{e} by \tilde{e}' and projecting it back to \mathcal{S} by ρ .

Every *Delaunay flip algorithm* takes as input a triangulation of \mathcal{S} and flips Delaunay-flippable edges (in any order) until there is none left. Every such algorithm terminates and outputs a Delaunay triangulation [7].

2.3 Mapping class group

We use the same notation as Maher [15] and refer to his paper for details.

The set $\text{Mod}(S_g)$ of all homeomorphisms (up to isotopy) of a topological surface S_g is called the *mapping class group* of S_g . Following Thurston's classification [10], $\text{Mod}(S_g)$ contains three kinds of elements: the periodic homeomorphisms, which are of finite order and are not useful for our purposes; the reducible ones, which fix at least one curve on S_g ; and the so-called *pseudo-Anosov* homeomorphisms, also known as the *hyperbolic* elements of $\text{Mod}(S_g)$.

104 Dehn twists (Figure 1, Left) are typical reducible elements, as they fix all the curves that do
 105 not intersect the curve used for twisting. A Dehn twist by a curve c at most adds to the length of
 106 a curve a constant that depends on the number of times the curve intersects c . A pseudo-Anosov
 107 element at most multiplies the length of a curve by a constant factor.

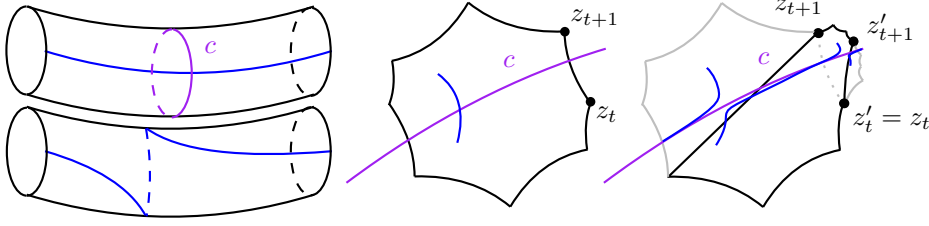


Figure 1: (Left) A Dehn twist along the curve c modifies the blue curve as shown. (Right) A t -twist on an admissible loosely-symmetric octagon.

108 $\text{Mod}(S_g)$ can be generated by a finite set of Dehn twists [9]. The composition of generators
 109 or their inverses in a random order can be interpreted as a random walk in $\text{Mod}(S_g)$: such a walk
 110 reaches pseudo-Anosov elements with asymptotic probability 1 [15]. However, this asymptotic
 111 result does not *a priori* describe the local structure of $\text{Mod}(S_g)$.

112 2.4 Admissible symmetric octagons

113 The Teichmüller space \mathcal{TM}_2 of the topological surface S_2 is the set of all the hyperbolic struc-
 114 tures (up to isotopy) that can be associated to S_2 . It admits various parametrizations. The
 115 most commonly used, though not well adapted to our needs, is the set of Fenchel-Nielsen coordi-
 116 nates [12, Section 7.6]. Here, we use a less usual set of parameters introduced by Aigon-Dupuy,
 117 Buser *et al.* [1], who proved that any surface of genus 2 has a fundamental domain that is an
 118 octagon in \mathbb{D} . This versatile representation allows us to easily construct and manipulate such
 119 surfaces in our experiments. In this section we recall some definitions and results of the original
 120 paper [1], following its notation.

121 Given $j \geq 3$ and complex numbers $z_1, \dots, z_j \in \mathbb{D}$ in convex position, $G[z_1, \dots, z_j]$ denotes the
 122 hyperbolic polygon whose vertices are z_1, \dots, z_j in this order. Given a compact subset $X \subset \mathbb{D}$,
 123 $\mathcal{A}(X)$ is the hyperbolic area of X . Given $z \in \mathbb{C}$, we denote by $\text{Re}[z]$ and $\text{Im}[z]$ its real and
 124 imaginary parts, respectively, by \bar{z} its conjugate, and by $|z|$ its modulus; i denotes a root of -1 .

125 Let $\arg z \in [0, 2\pi[$ denote the argument of a point $z \neq 0_{\mathbb{C}}$. Given $z_0, z_1, z_2, z_3 \in \mathbb{D} \setminus \{0_{\mathbb{C}}\}$, the
 126 4-tuple (z_0, z_1, z_2, z_3) is *valid* if $0 = \arg z_0 < \arg z_1 < \arg z_2 < \arg z_3 < \pi$; the hyperbolic octagon
 127 $\mathcal{P}[z_0, z_1, z_2, z_3]$ is then defined as $G[z_0, z_1, z_2, z_3, -z_0, -z_1, -z_2, -z_3]$. Such a hyperbolic octagon
 128 is called a *symmetric octagon*. The interior angles of a symmetric octagon cannot be greater than
 129 π . If moreover $\mathcal{A}(\mathcal{P}[z_0, z_1, z_2, z_3]) = 4\pi$, then $\mathcal{P}[z_0, z_1, z_2, z_3]$ and the 4-tuple (z_0, z_1, z_2, z_3) are
 130 called *admissible*. Each surface of genus 2 can be obtained by identifying the opposite sides of
 131 an admissible symmetric octagon [1]. Observe that the eight vertices of the octagon correspond
 132 to the same point on the surface.

133 A valid 4-tuple (z_0, z_1, z_2, z_3) is admissible if and only if $\text{Im} \left[\prod_{k=0}^3 (1 - z_k \bar{z}_{k+1}) \right] = 0$ [1,
 134 Lemma 3.2]. The authors establish this condition after proving a preliminary result that we
 135 will reuse: for any two points $z, z' \in \mathbb{D} \setminus \{0_{\mathbb{C}}\}$ if $0 \leq \arg z \leq \arg z' \leq \pi$ then [1, Appendix (A7)]

$$2 \arg(1 - z\bar{z}') = \mathcal{A}(G[0_{\mathbb{C}}, z, z']). \quad (1)$$

136 An admissible 4-tuple can be constructed as follows [1, Section 3]. Start with $z_1, z_2, z_3 \in \mathbb{D}$
 137 satisfying $0 < \arg(z_1) < \arg(z_2) < \arg(z_3) < \pi$. Abbreviate $u = (1 - z_1 \bar{z}_2)(1 - z_2 \bar{z}_3)$, $a =$
 138 $\text{Im}[-u \bar{z}_1 z_3]$, $b = \text{Im}[u(z_3 - \bar{z}_1)]$, and $c = \text{Im}[u]$. Assume $a + b + c < 0$ and let $z_0 = \frac{2c}{-b + \sqrt{b^2 - 4ac}}$.
 139 Then (z_0, z_1, z_2, z_3) is an admissible 4-tuple.

140 From now on indices are modulo 8. Let us consider an admissible 4-tuple (z_0, z_1, z_2, z_3)
 141 and define $z_{l+4} = -z_l$ for every $l \in \{0, 1, 2, 3\}$. For $k \in \{0, \dots, 7\}$, there exists a unique
 142 orientation preserving isometry $\tau_k : \mathbb{D} \rightarrow \mathbb{D}$ satisfying $\tau_k(z_{k+5}) = z_k$ and $\tau_k(z_{k+4}) = z_{k+1}$:
 143 the isometry τ_k maps a side of $\mathcal{P}[z_0, z_1, z_2, z_3]$ to the opposite side of $\mathcal{P}[z_0, z_1, z_2, z_3]$. Define
 144 $\omega_k = \frac{z_k(1 - |z_{k+1}|^2) + z_{k+1}(1 - |z_k|^2)}{1 - |z_k z_{k+1}|^2}$ and note that $|\omega_k| < 1$; the isometry τ_k is then given by
 145 $\tau_k(z) = (z + \omega_k)/(\bar{\omega}_k + 1)$ for every $z \in \mathbb{D}$ [1, Lemma 4.1]. Observe that $\tau_{k+4} = \tau_k^{-1}$.

146 3 Representation of triangulations

147 In this section we describe our data structure for representing triangulations (Section 3.1) and
 148 we sketch how it is maintained through flips (Section 3.2).

149 3.1 Data structure

150 Although an *ad hoc* data structure was previously proposed for flipping triangulations [7], we
 151 choose to use *combinatorial maps*, which are commonly used to represent graphs embedded on a
 152 surface. We refer the reader to the literature for a formal definition [16, Section 3.3]. The data
 153 structure we use offers a representation of the triangulation that intrinsically lies on the surface,
 154 while the earlier data structure [7, Section 4.1] stuck to specific representatives of all vertices
 155 and faces of the lifted triangulation in the universal cover. See Appendices A and B.1 for details
 156 on this section.

157 For our experiments, we use the flexible implementation of combinatorial maps that is publicly
 158 available in CGAL [5]. The *dart*, also known as *flag*, is the central object in a combinatorial map:
 159 it gives access to all incidence relations of an edge of the graph (Figure 2). In our setting a
 160 combinatorial map can be thought of as a halfedge data structure.

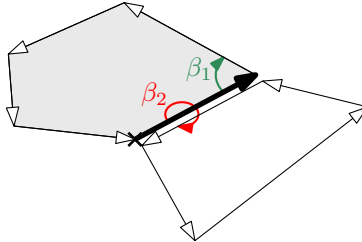


Figure 2: A dart in a combinatorial map (bold).

161 The geometric information for the triangulation is stored by adding a cross-ratio for each edge.
 162 Recall that the cross-ratio of four pairwise-distinct points in \mathbb{H} represented by $z_1, z_2, z_3, z_4 \in \mathbb{D}$
 163 is the complex number $[z_1, z_2, z_3, z_4] = \frac{(z_4 - z_2)(z_3 - z_1)}{(z_4 - z_1)(z_3 - z_2)}$ [3]. Cross-ratios are suitable for a
 164 flip algorithm, due to their well-known property: assuming that the four points are oriented
 165 counterclockwise, $\text{Im}[z_1, z_2, z_3, z_4] > 0$ if and only if z_4 lies inside the open disk circumscribing
 166 the triangle (z_1, z_2, z_3) .

167 Given an edge e of a triangulation T of \mathcal{S} we consider a lift $\tilde{e} = (\tilde{u}_1, \tilde{u}_3)$ of e in \mathbb{D} and the
 168 remaining vertices \tilde{u}_2 and \tilde{u}_4 of the two faces incident to \tilde{e} in \tilde{T} , numbering vertices counter-
 169 clockwise. The cross-ratio $\mathcal{R}_T(e)$ is defined as $[\tilde{u}_1, \tilde{u}_2, \tilde{u}_3, \tilde{u}_4]$; it is independent of the choice of
 170 the lift of e , as the cross-ratio is invariant under orientation preserving isometries of \mathbb{D} . An edge
 171 e of T is Delaunay-flippable if and only if $\text{Im}[\mathcal{R}_T(e)] > 0$.

172 Note that in our experiments, the lifts in \mathbb{D} are only used to calculate the cross-ratios of a
 173 given input triangulation T ; they are ignored during the flips, thus preserving the property that
 174 the data structure only considers the embedding of the triangulation on the surface. However,

175 in order to be able to recover a lift in \mathbb{D} in the end, e.g., for drawing a representation in \mathbb{D}
 176 of the final Delaunay triangulation, we need to maintain an *anchor* during flips. The anchor
 177 $A = (\delta, a_1, a_2, a_3)$ consists in a dart δ , chosen arbitrarily, together with a triple (a_1, a_2, a_3) of the
 178 vertices of a lift of the face containing δ .

179 A triangulation T is thus represented by (M, F, A) , where M is the combinatorial map, F
 180 the map that associates a cross-ratio to each edge of M , and $A = (\delta, a_1, a_2, a_3)$ is the anchor.

181 3.2 Flipping an edge

182 In this section, we quickly sketch how the data structure is maintained through an edge flip.
 183 First we modify the combinatorial map, then we update the anchor, and we finally update the
 184 cross-ratios. Some details and the pseudo-code are given in Appendix B.2.

185 Performing a flip in the combinatorial map is a straightforward use of the functionalities
 186 given by the CGAL package [5]. The triangulation obtained from T after flipping an edge e is
 187 denoted by T^* . By definition, the dart δ of the anchor A belongs to the face t of T represented
 188 by a lift $\tilde{t} = (a_1, a_2, a_3)$ in \mathbb{D} . If t does not contain e then A is not modified by the flip. However,
 189 if e is an edge of t then t will not belong to T^* and we must update A . A lift \tilde{e} of e incident to
 190 \tilde{t} is replaced by \tilde{e}^* when e is flipped. The anchor is updated so that it represents one of the two
 191 faces incident to \tilde{e}^* in T^* .

192 Finally, the cross-ratios must be retrieved. Only the cross-ratios of the at most 5 edges of
 193 the two triangles forming the quadrilateral whose diagonal is to be flipped must be updated.
 194 Their values after the flip are expressed in terms of their values before the flip (see Lemma 5 in
 195 Appendix A).

196 4 Solving arithmetic issues

197 The construction recalled in Section 2.4 shows that the real and imaginary parts of the complex
 198 numbers involved when defining surfaces are in general algebraic numbers. Efficiency issues when
 199 computing with algebraic numbers have been known for decades. More recently, they appeared
 200 when constructing Delaunay triangulations of hyperbolic surfaces [13, 8], showing that the hope
 201 to get effective software was restricted to very simple cases. In Section 4.1 we describe a simple
 202 experiment on the Bolza surface illustrating that these arithmetic issues are actually prohibitive
 203 in practice for the Delaunay flip algorithm in the sense that they imply unreasonable running
 204 times.

205 We show in Section 4.2 that any surface of genus 2 can be approximated by a surface de-
 206 scribed by rational numbers. It is straightforward to check that the computations made during
 207 a Delaunay flip algorithm only use the four basic operations $+$, $-$, \cdot , $/$ (see Section 3.2 and Ap-
 208 pendix B.2). Thus if the input surface is represented by rational numbers all numbers arising
 209 throughout the algorithm stay rational. This fact allows us to run extensive experiments.

210 4.1 Issues when using algebraic numbers

211 Let $c_k = \frac{\exp(i\pi \frac{2k-1}{8})}{2^{1/4}}$, $k \in \{0, \dots, 7\}$ be the vertices of a regular hyperbolic octagon in \mathbb{D} ;
 212 identifying the opposite sides of this octagon gives a surface of genus 2 known as the Bolza
 213 surface. Consider the triangulation T_0 of the octagon shown in Figure 3. Identifying in T_0
 214 the edges corresponding to opposite sides of the octagon yields a triangulation T of the Bolza
 215 surface. Let e_0, \dots, e_4 be the edges of T corresponding to the edges e'_0, \dots, e'_4 of T_0 . The algebraic
 216 numbers $\cos\left(\frac{\pi}{8}\right) = \frac{\sqrt{2+\sqrt{2}}}{2}$ and $\sin\left(\frac{\pi}{8}\right) = \frac{\sqrt{2-\sqrt{2}}}{2}$ naturally appear when computing the
 217 cross-ratios $\mathcal{R}_T(e_l) = [c_0, c_{l+1}, c_{l+2}, c_{l+3}]$, $l \in \{0, \dots, 4\}$.

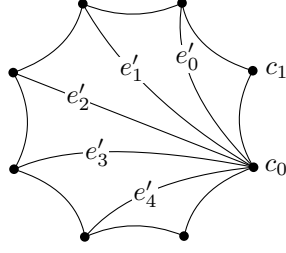


Figure 3: The triangulation T_0 and the edges e'_0, \dots, e'_4 .

218 As the points $c_k, k = 0, \dots, 7$ are concyclic e_0, \dots, e_4 can be flipped although they are strictly
 219 speaking not Delaunay-flippable: the situation is degenerate. The experiment consists in com-
 220 puting the new values of the cross-ratios involved during the flips of e_0, \dots, e_4 in this order (see
 221 Appendix C.1 for the pseudocode). We used the CGAL wrapper `CORE::Expr` [11] for the algebraic
 222 numbers provided by the CORE library [18]. It took minutes to finish on an Intel Core i5-8250u
 223 cpu (1.6Ghz, 8 cores) and 16Gb of ram. Such a running time severely restricts the possibility to
 224 run heavy experiments with a Delaunay flip algorithm.

225 4.2 Density of the rationally described surfaces

226 For any $z \in \mathbb{D}$ and any $\varepsilon > 0$, $B(z, \varepsilon)$ denotes the open ball $\{z' \in \mathbb{D} : d(z, z') < \varepsilon\}$ where $d(\cdot, \cdot)$
 227 is the hyperbolic distance in \mathbb{D} .

228 **Definition 1.** We say that a 4-tuple (z_0, z_1, z_2, z_3) is *rational* if $z_k \in \mathbb{Q} + i\mathbb{Q}$ for every $k \in$
 229 $\{0, 1, 2, 3\}$. A *rationally described surface* is a surface obtained from a rational admissible 4-
 230 tuple $(\mathbf{z}_0, \mathbf{z}_1, \mathbf{z}_2, \mathbf{z}_3)$ by identifying the opposite sides of $\mathcal{P}[\mathbf{z}_0, \mathbf{z}_1, \mathbf{z}_2, \mathbf{z}_3]$.

231 **Theorem 2.** Let (z_0, z_1, z_2, z_3) be an admissible 4-tuple and $\varepsilon > 0$. There exists a rational
 232 admissible 4-tuple $(\mathbf{z}_0, \mathbf{z}_1, \mathbf{z}_2, \mathbf{z}_3)$ such that $\forall k \in \{0, 1, 2, 3\}, \mathbf{z}_k \in B(z_k, \varepsilon)$.

233 *Proof.* For two reals a and b , define $]a, b[= \{z \in \mathbb{C} : a < \operatorname{Re}[z] < b \text{ and } \operatorname{Im}[z] = 0\}$. We first
 234 choose for every $k \in \{0, 1, 2, 3\}$ a point $\mathbf{z}_k \in B(z_k, \varepsilon) \cap (\mathbb{Q} + i\mathbb{Q})$, with the additional requirement
 235 that $\mathbf{z}_0 \in]0, 1[$, but without trying to satisfy the area condition $\mathcal{A}(G[-\mathbf{z}_0, \mathbf{z}_0, \mathbf{z}_1, \mathbf{z}_2, \mathbf{z}_3]) = 2\pi$
 236 (equivalent to the condition $\mathcal{A}(\mathcal{P}[z_0, z_1, z_2, z_3]) = 4\pi$ given in Section 2.4). Consider Figure 4.
 237 If ε is small enough, then $(\mathbf{z}_0, \mathbf{z}_1, \mathbf{z}_2, \mathbf{z}_3)$ is valid. We will now show that if each \mathbf{z}_k is "close
 238 enough" to z_k for every k , we can replace \mathbf{z}_3 by a point U in $B(z_3, \varepsilon) \cap (\mathbb{Q} + i\mathbb{Q})$ so that the area
 239 condition is satisfied. More details on the construction can be found in Appendix C.2.

240 To do so we first define an isometry $\mathbf{f} : \mathbb{D} \rightarrow \mathbb{D}$ in the Poincaré disk: $\mathbf{f}(z) = \frac{z + \mathbf{z}_0}{\mathbf{z}_0 z + 1}$. Observe
 241 that $\mathbf{f}(-\mathbf{z}_0) = 0_{\mathbb{C}}$. Since \mathbf{f} and \mathbf{f}^{-1} both map $\mathbb{D} \cap (\mathbb{Q} + i\mathbb{Q})$ to some subset of $\mathbb{D} \cap (\mathbb{Q} + i\mathbb{Q})$
 242 our problem reduces to replacing $\mathbf{f}(\mathbf{z}_3)$ by an element V of $B(\mathbf{f}(z_3), \varepsilon) \cap (\mathbb{Q} + i\mathbb{Q})$ satisfying
 243 $\mathcal{A}(G[0_{\mathbb{C}}, \mathbf{f}(\mathbf{z}_0), \mathbf{f}(\mathbf{z}_1), \mathbf{f}(\mathbf{z}_2), V]) = 2\pi$. Indeed, by setting $U = \mathbf{f}^{-1}(V)$ we obtain $U \in B(z_3, \varepsilon) \cap$
 244 $(\mathbb{Q} + i\mathbb{Q})$ and $\mathcal{A}(G[-\mathbf{z}_0, \mathbf{z}_0, \mathbf{z}_1, \mathbf{z}_2, U]) = \mathcal{A}(G[0_{\mathbb{C}}, \mathbf{f}(\mathbf{z}_0), \mathbf{f}(\mathbf{z}_1), \mathbf{f}(\mathbf{z}_2), V]) = 2\pi$.

To find such a point V , we define a polynomial $P \in \mathbb{Q}[X]$ by setting

$$P(X) = \operatorname{Im} \left[(1 - \mathbf{f}(\mathbf{z}_0) \overline{\mathbf{f}(\mathbf{z}_1)}) (1 - \mathbf{f}(\mathbf{z}_1) \overline{\mathbf{f}(\mathbf{z}_2)}) (1 - X \mathbf{f}(\mathbf{z}_2) \overline{\mathbf{f}(\mathbf{z}_3)}) \right].$$

245 Observe that the degree of P is at most 1, and thus $P(X) = (P(1) - P(0))X + P(0)$. We first
 246 show that if we choose \mathbf{z}_k close to z_k for every $k \in \{0, 1, 2, 3\}$, $P(1)$ is close to 0 and $P(0)$ close
 247 to $\kappa > 0$. Since $0 = \arg \mathbf{f}(\mathbf{z}_0) < \arg \mathbf{f}(\mathbf{z}_1) < \arg \mathbf{f}(\mathbf{z}_2) < \arg \mathbf{f}(\mathbf{z}_3) < \pi$ we can apply Equality (1)

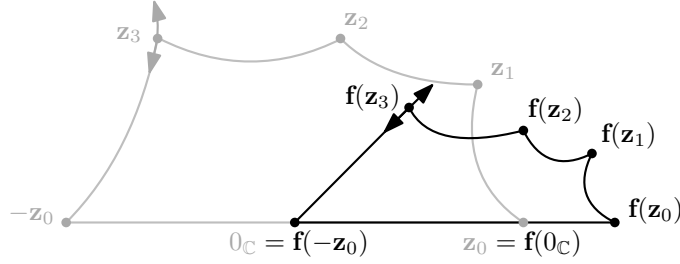


Figure 4: Illustration of the proof of Theorem 2

248 and obtain

$$\begin{aligned}
 & \arg \left[\left(1 - \mathbf{f}(\mathbf{z}_0)\overline{\mathbf{f}(\mathbf{z}_1)}\right) \left(1 - \mathbf{f}(\mathbf{z}_1)\overline{\mathbf{f}(\mathbf{z}_2)}\right) \left(1 - \mathbf{f}(\mathbf{z}_2)\overline{\mathbf{f}(\mathbf{z}_3)}\right) \right] \\
 &= \arg \left(1 - \mathbf{f}(\mathbf{z}_0)\overline{\mathbf{f}(\mathbf{z}_1)}\right) + \arg \left(1 - \mathbf{f}(\mathbf{z}_1)\overline{\mathbf{f}(\mathbf{z}_2)}\right) + \arg \left(1 - \mathbf{f}(\mathbf{z}_2)\overline{\mathbf{f}(\mathbf{z}_3)}\right) \\
 &= \frac{1}{2} [\mathcal{A}(G[0_{\mathbb{C}}, \mathbf{f}(\mathbf{z}_0), \mathbf{f}(\mathbf{z}_1)]) + \mathcal{A}(G[0_{\mathbb{C}}, \mathbf{f}(\mathbf{z}_1), \mathbf{f}(\mathbf{z}_2)]) + \mathcal{A}(G[0_{\mathbb{C}}, \mathbf{f}(\mathbf{z}_2), \mathbf{f}(\mathbf{z}_3)])] \\
 &= \frac{1}{2} \mathcal{A}(G[0_{\mathbb{C}}, \mathbf{f}(\mathbf{z}_0), \mathbf{f}(\mathbf{z}_1), \mathbf{f}(\mathbf{z}_2), \mathbf{f}(\mathbf{z}_3)]) = \frac{1}{2} \mathcal{A}(G[-\mathbf{z}_0, \mathbf{z}_0, \mathbf{z}_1, \mathbf{z}_2, \mathbf{z}_3]).
 \end{aligned}$$

249 By observing that every expression in between the equalities belongs to $[0, 2\pi[$ we see that those
 250 equalities are indeed equalities and not only congruences modulo 2π . By choosing \mathbf{z}_k close to
 251 z_k for every $k \in \{0, 1, 2, 3\}$ we make the last expression approach $\frac{1}{2} \mathcal{A}(G[-z_0, z_0, z_1, z_2, z_3]) = \pi$,
 252 which makes $P(1)$ tend to 0. Similarly, we obtain

$$\arg \left[\left(1 - \mathbf{f}(\mathbf{z}_0)\overline{\mathbf{f}(\mathbf{z}_1)}\right) \left(1 - \mathbf{f}(\mathbf{z}_1)\overline{\mathbf{f}(\mathbf{z}_2)}\right) \right] = \frac{1}{2} \mathcal{A}(G[-\mathbf{z}_0, \mathbf{z}_0, \mathbf{z}_1, \mathbf{z}_2]).$$

253 By choosing \mathbf{z}_k closer and closer to z_k , the last expression tends to $\frac{1}{2} \mathcal{A}(G[-z_0, z_0, z_1, z_2])$ which
 254 is not congruent to 0 modulo π . Thus $P(0)$ is close to some constant $\kappa > 0$, whence we can
 255 assume that $P(1) \neq P(0)$.

256 To construct V set $\lambda = \frac{P(0)}{P(0)-P(1)}$ and let $V = \lambda \mathbf{f}(\mathbf{z}_3)$; we have both $V \in \mathbb{Q} + i\mathbb{Q}$ and
 257 $P(\lambda) = 0$. We proved that $P(1)$ tends to 0 and that $P(0)$ tends to $\kappa > 0$ so λ tends to 1 and V
 258 tends to $\mathbf{f}(\mathbf{z}_3)$. Finally, observe that $P(\lambda) = 0$ implies $\mathcal{A}(G[0_{\mathbb{C}}, \mathbf{f}(\mathbf{z}_0), \mathbf{f}(\mathbf{z}_1), \mathbf{f}(\mathbf{z}_2), V]) = 2\pi$ by
 259 Equality (1). \square

260 *Remark 3.* This theorem implies the density of the hyperbolic structures corresponding to ratio-
 261 nal admissible 4-tuples in \mathcal{TM}_2 with its canonical topology. However, a proof would go beyond
 262 the scope of this paper and would be quite technical.

263 5 The generation of the input for the experiments

264 We generate input for the Delaunay flips algorithms by triangulating admissible loosely-symmetric
 265 octagons; the latter are defined in Section 5.1 as a slight extension of the admissible symmetric
 266 octagons (Section 2.4). We generate such octagons whose vertices are represented in \mathbb{D} by
 267 complex numbers with rational real and imaginary parts. To conduct experiments, we need to
 268 generate a large number of triangulations with a large diameter. An effective approach consists
 269 in generating octagons with a small diameter and twisting them (Section 5.1) many times to
 270 obtain octagons with a very large diameter. This approach has two advantages. Firstly it can
 271 generate triangulations with different diameters but lying on a single surface, hence eliminating
 272 any dependency on the choice of the surface if needed. Secondly thanks to this approach we will
 273 also study the dependency of the number of flips on those twists.

274 5.1 The twists of admissible loosely-symmetric octagons

275 We say that a hyperbolic octagon P is *loosely-symmetric* if the opposite sides of P are isometric
 276 and the opposite interior angles of P are equal. If moreover $\mathcal{A}(P) = 4\pi$ then we call P *admissible*.
 277 Clearly, the symmetric octagons of Aigon-Dupuy *et al.* (Section 2.4) are loosely-symmetric
 278 octagons. Identifying the opposite sides of an admissible loosely-symmetric octagon gives a
 279 surface of genus 2 [4, Theorem 1.3.5].

280 Let $G[z_0, \dots, z_7]$ be an admissible loosely-symmetric octagon. We will consider the Dehn
 281 twists along the axes of its side-pairings (Figure 1). These twists generate a subgroup of $\text{Mod}(S_2)$
 282 (Section 2.3), which contains non-reducible elements of $\text{Mod}(S_2)$ since the generators do not all
 283 fix a common curve. Thus, this subgroup contains pseudo-Anosov elements [14].

For every $k \in \{0, \dots, 7\}$ we denote by τ_k the orientation preserving isometry of \mathbb{D} that satisfies
 $\tau_k(z_{k+5}) = z_k$ and $\tau_k(z_{k+4}) = z_{k+1}$. We fix $t \in \{0, \dots, 7\}$. For $k \in \{0, \dots, 7\}$ let

$$z'_k = \begin{cases} \tau_t(z_k) & \text{if } k - t \in \{1, 2, 3, 4\} \pmod{8}, \\ z_k & \text{otherwise.} \end{cases}$$

284 By the Gauss-Bonnet formula, the interior angles of $G[z_0, \dots, z_7]$ sum up to 2π ; since opposite
 285 interior angles are equal, each interior angle is at most π . Thus the geodesic segment between z_{t+1}
 286 and z_{t+5} is contained in $G[z_0, \dots, z_7]$ and cuts the polygon into the two interior disjoint pentagons
 287 $P_1 = G[z_{t+1}, z_{t+2}, z_{t+3}, z_{t+4}, z_{t+5}]$ and $P_2 = G[z_{t+5}, z_{t+6}, z_{t+7}, z_t, z_{t+1}]$; the intersection of P_1 and
 288 P_2 is the segment between z_{t+5} and z_{t+1} and the two pentagons are isometric. Similarly, $\tau_t(P_1)$
 289 and P_2 are interior disjoint, they intersect on the segment between $z'_t = z_t$ and $z'_{t+4} = z_{t+1}$
 290 and their union is $G[z'_0, \dots, z'_7]$. It follows that $G[z'_0, \dots, z'_7]$ is an admissible loosely-symmetric
 291 octagon; the surface that it defines is isometric to the one defined by $G[z_0, \dots, z_7]$ as both can
 292 be obtained by the same identification of the sides of P_1 and P_2 (P_1 and $\tau_t(P_1)$ being isometric).
 293 We say that (z'_0, \dots, z'_7) is obtained by *t-twisting* (z_0, \dots, z_7) . For every point z in the closure
 294 of $G[z_0, \dots, z_7]$ at least z or $\tau_t(z)$ lies in the closure of $G[z'_0, \dots, z'_7]$.

Let us denote by $(\tau'_k)_{0 \leq k \leq 7}$ the isometries defined for z'_0, \dots, z'_7 , in the same way as $(\tau_k)_{0 \leq k \leq 7}$
 above. By definition of the *t-twist*, the following holds for every $k \in \{0, \dots, 7\}$

$$\tau'_k = \begin{cases} \tau_t \circ \tau_k & \text{if } k - t \in \{1, 2, 3\} \pmod{8}, \\ \tau_k \circ \tau_t^{-1} & \text{if } t - k \in \{1, 2, 3\} \pmod{8}, \\ \tau_k & \text{if } k = t \pmod{4}. \end{cases}$$

295 For a word $t = t_1 \cdots t_m$, we define the *t-twist* as the composition of the t_k -twists, $k = 1, \dots, m$,
 296 in this order. We pick t_1, \dots, t_m in $\{0, \dots, 3\}^m$ instead of $\{0, \dots, 7\}^m$ to only consider the
 297 generators without their inverses and obtain large diameters as quickly as possible.

298 5.2 The generation of triangulations

299 The input surfaces and triangulations are constructed in four steps. We refer to Appendix D for
 300 details.

3[step 1] We construct an initial rational admissible 4-tuple $(\mathbf{z}_0, \mathbf{z}_1, \mathbf{z}_2, \mathbf{z}_3)$.

3[step 2] We choose $n_p \geq 0$ and construct points $(\mathbf{p}_1, \dots, \mathbf{p}_{n_p}) \in (\mathbb{Q} + i\mathbb{Q})^n$ lying within the closure
 303 of $\mathcal{P}[\mathbf{z}_0, \mathbf{z}_1, \mathbf{z}_2, \mathbf{z}_3]$.

3[step 3] We choose $m \geq 0$ and a sequence $t_1 \cdots t_m$ of twists.

3[step 4] From the 4-tuple $(\mathbf{z}_0, \mathbf{z}_1, \mathbf{z}_2, \mathbf{z}_3)$, the points $(\mathbf{p}_1, \dots, \mathbf{p}_{n_p})$, and the sequence $t = t_1 \cdots t_m$,
 306 we construct a representation (M, F, A) of an input triangulation T . This is (roughly)
 307 done by *t-twisting* $\mathcal{P}[\mathbf{z}_0, \mathbf{z}_1, \mathbf{z}_2, \mathbf{z}_3]$, triangulating the octagon resulting from the twists,
 308 and inserting the points in the faces of the resulting triangulation. Together with the point
 309 corresponding to the vertices of the octagon, the triangulation T has $n = n_p + 1$ vertices.

Sections 6 and 7 refer to these four steps. Step 1 was applied a thousand times to construct the 1,000 rational admissible 4-tuples $Q_1, \dots, Q_{1,000}$; in our experiments we consider the first n_q 4-tuples. In step 3 we constructed 10,000 random sequences of twists denoted by $S_1, \dots, S_{10,000}$, each of length 10, of which some of the experiments use the first n_s sequences. The values of n_p, n_q , and n_s are specified in the description of each experiment.

Technicalities for steps 1, 2, and 4 are deferred to Appendix D. We only elaborate on step 3 here. Consider a sequence of m twists represented by the word $t = t_1 \dots t_m$ (see Section 5.1). We will study two kinds of sequences in the experiments of Sections 6 and 7:

- A *power sequence* is represented by a word u^m for some $u \in \{0, \dots, 3\}$.
- In a *random sequence*, t_1, \dots, t_m are chosen uniformly and independently in $\{0, \dots, 3\}$.

It appears in practice that the length of a random sequence has a stronger impact on the computations than the length of a power sequence. When twisting, we update an 8-tuple $(\mathbf{z}_0, \dots, \mathbf{z}_7) \in (\mathbb{Q} + i\mathbb{Q})^8$ corresponding to an admissible loosely-symmetric octagon $G[\mathbf{z}_0, \dots, \mathbf{z}_7]$, together with the orientation preserving isometries $(\tau_k)_{0 \leq k \leq 7}$ identifying its opposite sides. Both the vertices of the octagon and the isometries are represented by complex numbers: $8(m+1)$ complex numbers for the $8(m+1)$ points and $32(m+1)$ complex numbers for the $8(m+1)$ isometries. Each such complex number is represented by two rational numbers and each such rational number is represented by two integers: its numerator and its denominator. The running time of a sequence of $m \geq 0$ twists thus depends on the sizes of these $160(m+1)$ integers; here the size of an integer is the number of digits of its decimal representation.

Twisting promptly gives rise to big numbers. As an example, take the rational admissible 4-tuple $\mathbf{z}_0 = 10/11, \mathbf{z}_1 = 1/2 + 1/2i, \mathbf{z}_2 = -1/10 + 9/10i, \mathbf{z}_3 = -3/5 + 3/5i$. Then twist $(\mathbf{z}_0, \dots, \mathbf{z}_3, -\mathbf{z}_0, \dots, -\mathbf{z}_3)$ by m twists and get $(\mathbf{z}_{0,m}, \dots, \mathbf{z}_{7,m}) \in (\mathbb{Q} + i\mathbb{Q})^8$ such that $G[\mathbf{z}_{0,m}, \dots, \mathbf{z}_{7,m}]$ is an admissible loosely-symmetric octagon. Denote by $\tau_{k,m}$ the orientation preserving isometry of \mathbb{D} mapping $\mathbf{z}_{k+5,m}$ to $\mathbf{z}_{k,m}$ and $\mathbf{z}_{k+4,m}$ to $\mathbf{z}_{k+1,m}$, for $k \in \{0, \dots, 7\}$.

Consider first the power sequence of twists 0^m (the choice of 0 is without loss of generality) for $m \in \{0, \dots, 3000\}$. A simple recursion gives the following for every m :

$$\tau_{k,m} = \begin{cases} (\tau_{0,0})^m \circ \tau_{k,0} & \text{if } k \in \{1, 2, 3\} \pmod{8} \\ \tau_{k,0} \circ (\tau_{0,0})^{-m} & \text{if } k \in \{5, 6, 7\} \pmod{8} \\ \tau_{k,0} & \text{if } k = 0 \pmod{4} \end{cases}$$

$$\mathbf{z}_{k,m} = \begin{cases} (\tau_{0,0})^m(\mathbf{z}_{k,0}) & \text{if } k \in \{1, 2, 3\} \pmod{8}, \\ \mathbf{z}_{k,0} & \text{otherwise.} \end{cases}$$

From that it is easy to see that the sizes of the integers involved in the representations of $(\tau_{k,m})_{0 \leq k \leq 7}$ and $(\mathbf{z}_{k,m})_{0 \leq k \leq 7}$ grow at most linearly in m . See Figure 5.

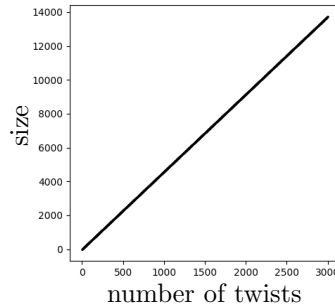


Figure 5: Size of the numerator of $\text{Re}[z_{1,m}]$ as a function of the length m of a power sequence of twists.

337 When twisting with a random sequence, the growth in size of the integers involved does not
 338 appear to be linear in the number of twists. Examples are shown in Figure 6 for the random
 339 sequence 23330132013121032301 of $m = 20$ twists. Observe that the numerator of the real part
 340 of the top-left coefficient of the matrix representing $\tau_{0,20}$ contains more than 200,000 digits in
 341 its decimal representation. In general the bottleneck for such computations seems to be the size
 342 of such coefficients of the isometries $(\tau_{k,m})_{0 \leq k \leq 7}$.

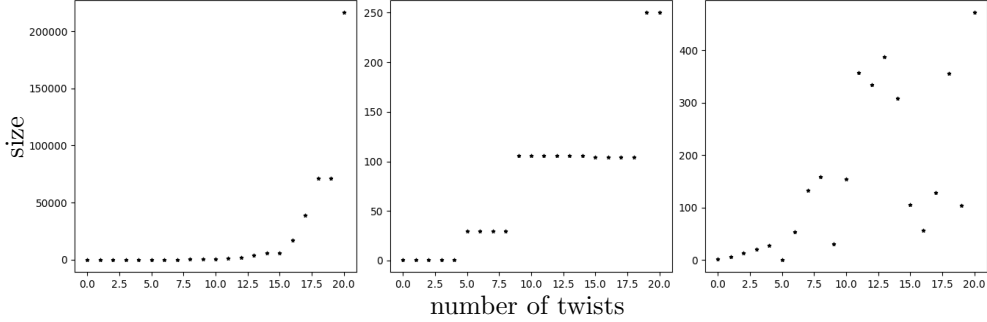


Figure 6: The size of integers as a function of the length m of a random sequence of twists. Left: the numerator of the real part of the top-left coefficient of the matrix representation of $\tau_{0,m}$. Middle: the numerator of $\text{Re}[z_{1,m}]$. Right: the numerator of $\text{Re}[z_{4,m}]$.

343 6 Comparison of flip strategies

344 As recalled in Section 2.2, a Delaunay flip algorithm can flip Delaunay-flippable edges in any
 345 order. In this section, we consider six strategies:

- 346 • *naive* strategy: choose the first Delaunay-flippable edge given by the CGAL combinatorial
 347 map iterator `DartRange::iterator`.
- 348 • *random* strategy: choose uniformly among all the Delaunay-flippable edges.
- 349 • *minimag* and *maximag* strategies: choose the edge e whose cross-ratio $\mathcal{R}_T(e)$ minimizes
 350 (resp. maximizes) $\text{Im}[\mathcal{R}_T(e)]$ among the Delaunay-flippable edges.
- 351 • *minratio* and *maxratio* strategies: choose the edge e whose cross-ratio $\mathcal{R}_T(e)$ minimizes
 352 (resp. maximizes) the quotient $|\text{Im}[\mathcal{R}_T(e)]| / |\mathcal{R}_T(e)|$.

353 We present eight experiments A, B, C, D, E, F, G, and H, allowing us to compare the
 354 number of flips that the six strategies induce on a variety of inputs. The notation Q_k , S_k and
 355 the parameters n_q , n_s , and n_p are defined in Section 5.

exp.	A	B	C	D	exp.	E	F	G	H
n_q	50	30	10	1	n_q	100	30	10	10
n_s	50	30	10	10	Ω	0, 30, 60, 90, 120	0, 30, 60, 90, 120	0, 10, 20, 30	0, 5, 10
n_p	0	10	100	1,000	n_p	0	10	100	1,000

Table 1: Parameters for experiments A to H.

356 Let us first check that the strategy actually has an influence on the number of flips. Experi-
 357 ments A, B, C, and D use random sequences of twists. The values of n_q , n_s , and n_p are shown
 358 in Table 1. We first construct the set X containing the 11 prefixes of the sequence of twists S_l
 359 (including the empty sequence) for every $l \in \{1, \dots, n_s\}$: X contains at most $10n_s + 1$ sequences

360 whose sizes vary between 0 and 10. Then for every $k \in \{1, \dots, n_q\}$ and every $t \in X$, we perform
 361 steps 2 and 4 with $(\mathbf{z}_0, \mathbf{z}_1, \mathbf{z}_2, \mathbf{z}_3) = Q_k$, n_p interior vertices, and $t_1 \cdots t_m = t$. In each case, we
 362 run the Delaunay flip algorithm six times: one for each strategy, and count the number of flips
 363 that were needed for the algorithm to terminate. Among those six integers we denote by $\alpha_{k,t}$ the
 364 minimum and by $\beta_{k,t}$ the maximum. Figure 7 shows that choosing a strategy has an impact on
 365 the number of flips. A point lying far from the diagonal $y = x$ represents a computation where
 366 one of the strategies clearly requires more flips than another, while a point lying close to the
 367 diagonal represents a computation where the strategies were essentially equivalent in the number
 368 of flips they induced.

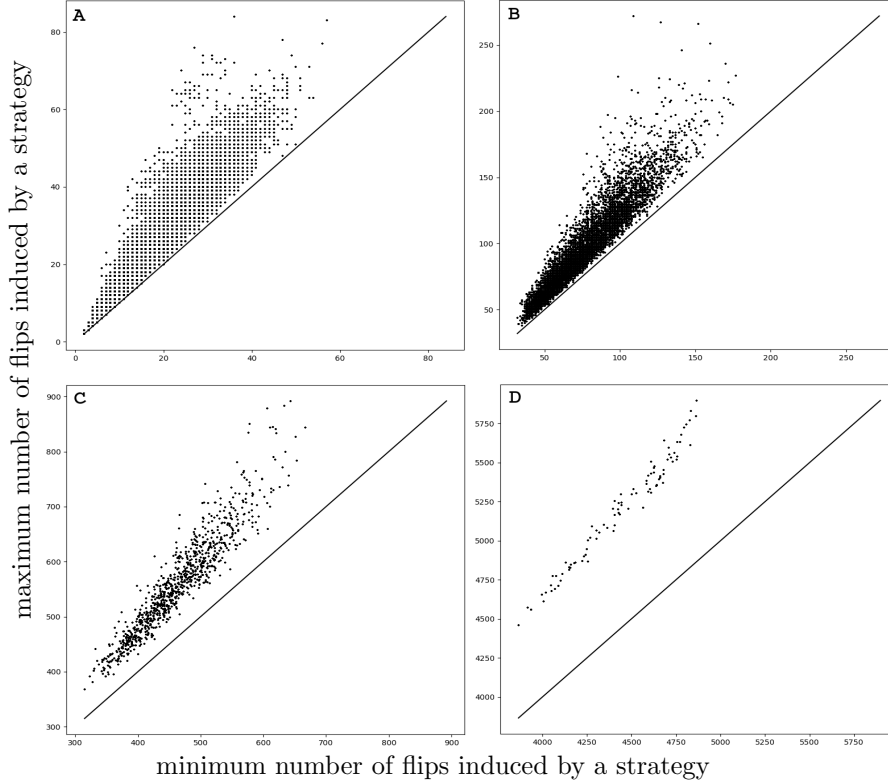


Figure 7: Experiments A, B, C, and D: points $(\alpha_{k,t}, \beta_{k,t})$ for $k \in \{1, \dots, n_q\}$ and $t \in X$.

369 Experiments E, F, G, and H use power sequences of twists. They are parameterized by
 370 n_q, n_p , and a set Ω of integers giving the lengths of the considered twists, see Table 1. For
 371 every $k \in \{1, \dots, n_q\}$, every $m \in \Omega$, and every $u \in \{0, 1, 2, 3\}$, we perform steps 2 and 4 with
 372 $(\mathbf{z}_0, \mathbf{z}_1, \mathbf{z}_2, \mathbf{z}_3) = Q_k$, n_p interior vertices, and $t_1 \dots t_m = u^m$. Then we run the Delaunay flip
 373 algorithm for each of the six strategies. Here, the minimum and maximum number of flips are
 374 respectively denoted by $\alpha_{k,m,u}$ and $\beta_{k,m,u}$. Figure 8 shows a stronger impact of the strategy on
 375 the number of flips than experiments A, B, C, D.

376 To compare the six strategies, we count for each experiment and each strategy the number
 377 of times (i.e., the number of pairs $(\alpha_{k,t}, \beta_{k,t})$ for experiments A, \dots , D or pairs $(\alpha_{k,m,u}, \beta_{k,m,u})$
 378 for experiments E, \dots , H) when the strategy induced the minimum/maximum number of flips
 379 among the other strategies. Figure 9 summarizes the results. Overall the minratio and the
 380 maxratio strategies seem to regularly achieve the maximum and the minimum (respectively).
 381 Observe in particular that in experiments D and H the minratio and the maxratio strategies
 382 *always* induced more and fewer flips, respectively, than any other strategy.

383 The naive strategy seems to rarely achieve the minimum or the maximum number of flips
 384 among the six strategies. In Figures 10 and 11, the y -coordinate is the number of flips induced
 385 by the naive strategy (instead of the maximum among the six strategies); the x -coordinate is

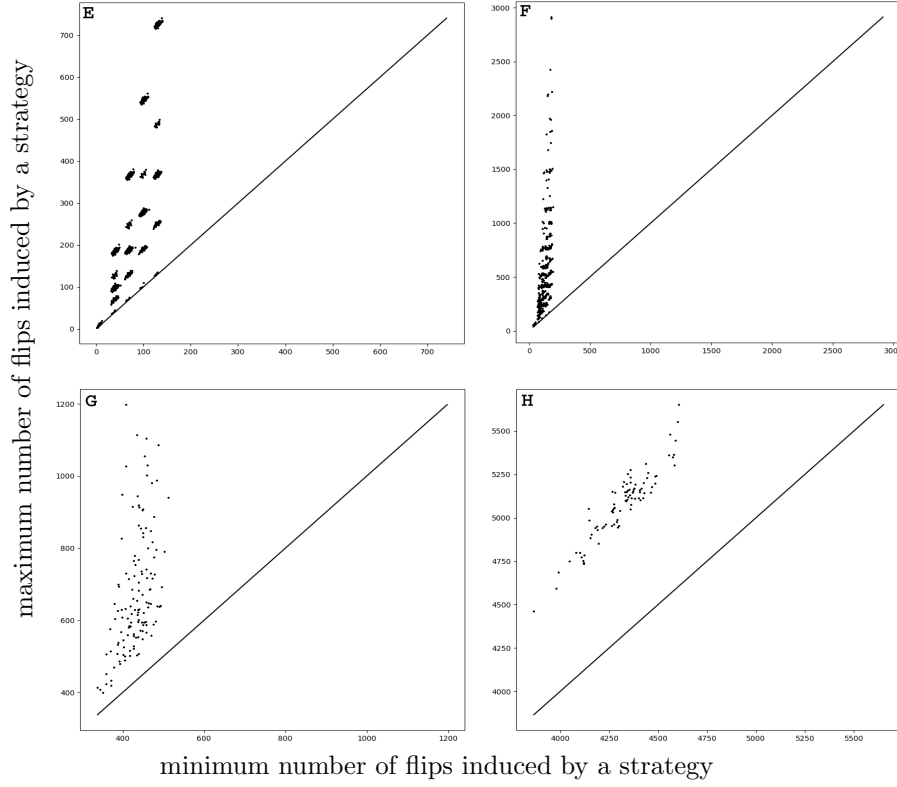


Figure 8: Experiments E, F, G, and H: points $(\alpha_{k,m,u}, \beta_{k,m,u})$, $k \in \{1, \dots, n_q\}, m \in \Omega, u \in \{0, 1, 2, 3\}$.

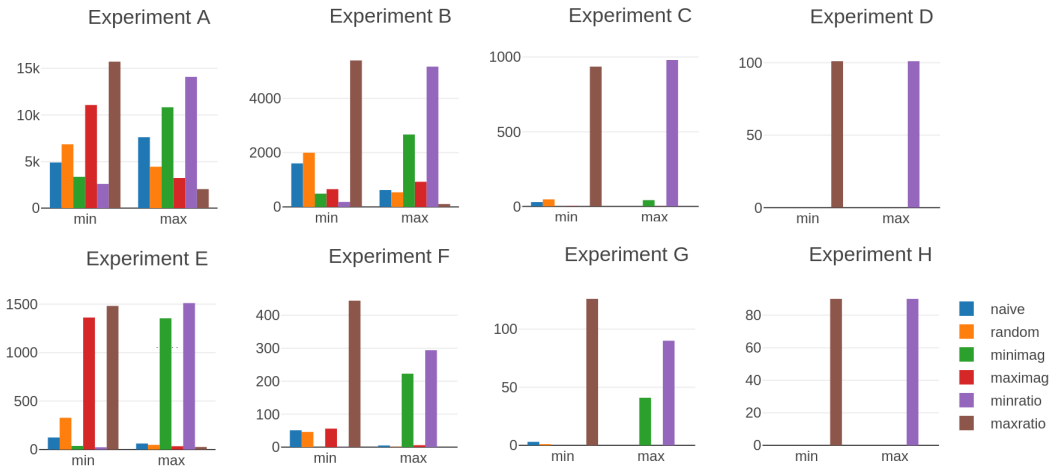


Figure 9: The number of times when each strategy induced the minimum/maximum number of flips.

386 still the minimum number of flips among the six strategies. The figures show that the number
 387 of flips required by the naive strategy is close to the minimum. As it runs much faster than all
 388 other strategies, we stick to the naive strategy for the experiments of Section 7.

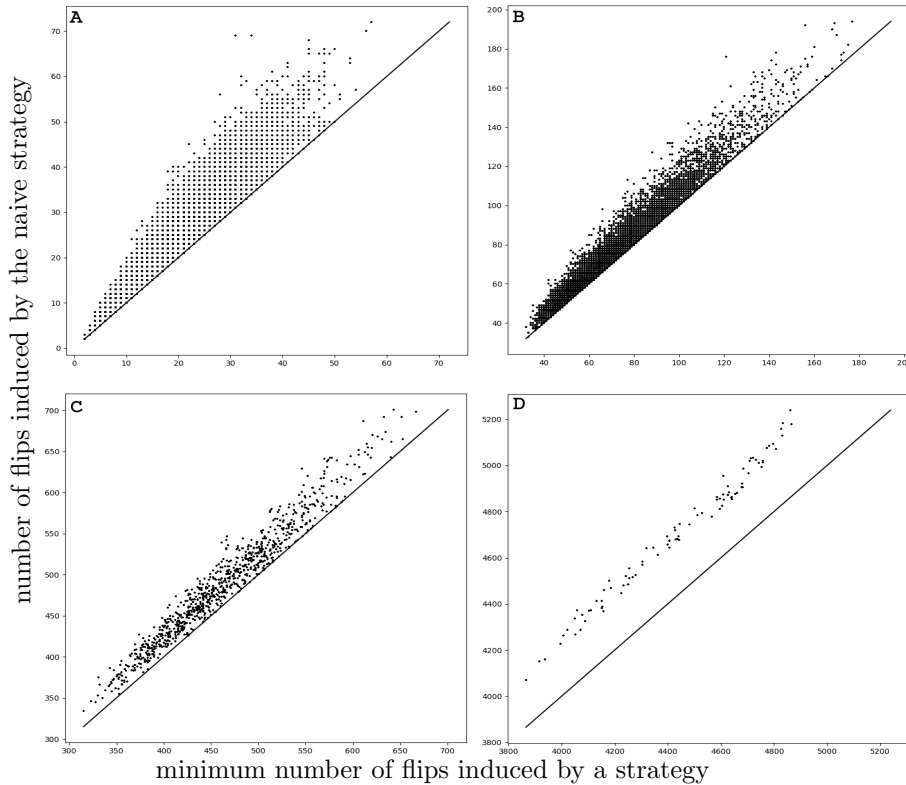


Figure 10: The number of flips induced by the naive strategy with respect to the minimum among the six strategies in experiments A, B, C, and D.

389 Figure 12 illustrates a run of the program. The diameter of the initial domain is about 139
 390 and the diameter of the final domain is smaller than 5.

391 7 Exploring the relationship between number of flips and diam- 392 eter

393 7.1 Rationale for the experiments

394 Mark Bell [2] showed that the structure of the mapping class group has a very interesting effect
 395 on the flip graph of topological triangulations. In this topological setting, the objective is to
 396 reduce the number of intersections k of the input triangulation with a fixed curve. The main
 397 theorem of Bell's paper states that one can always find a flip or a power of a Dehn twist that
 398 reduces the number of crossings by a fixed percentage. This result can be seen as follows: either a
 399 pseudo-Anosov transformation allows the number of crossings to decrease in a single application,
 400 or there exists a power of a Dehn twist that reduces the number of crossings. This gives an
 401 algorithm to compute the optimal triangulation using $O(\log(k))$ operations.

402 Our problem is different from Mark Bell's: in his study, the number of crossings is an explicit
 403 measure of the distance to the goal, while there is no way to know in advance how far the input
 404 triangulation is from being Delaunay, and we do not know the homotopy classes of final edges.
 405 However, asymptotically, combinatorial intersection metrics are very similar to the hyperbolic
 406 metrics on surfaces of genus $g \geq 2$. If a triangulation has very long edges (in terms of the
 407 number of crossings for the topological version, or in terms of the hyperbolic length in our

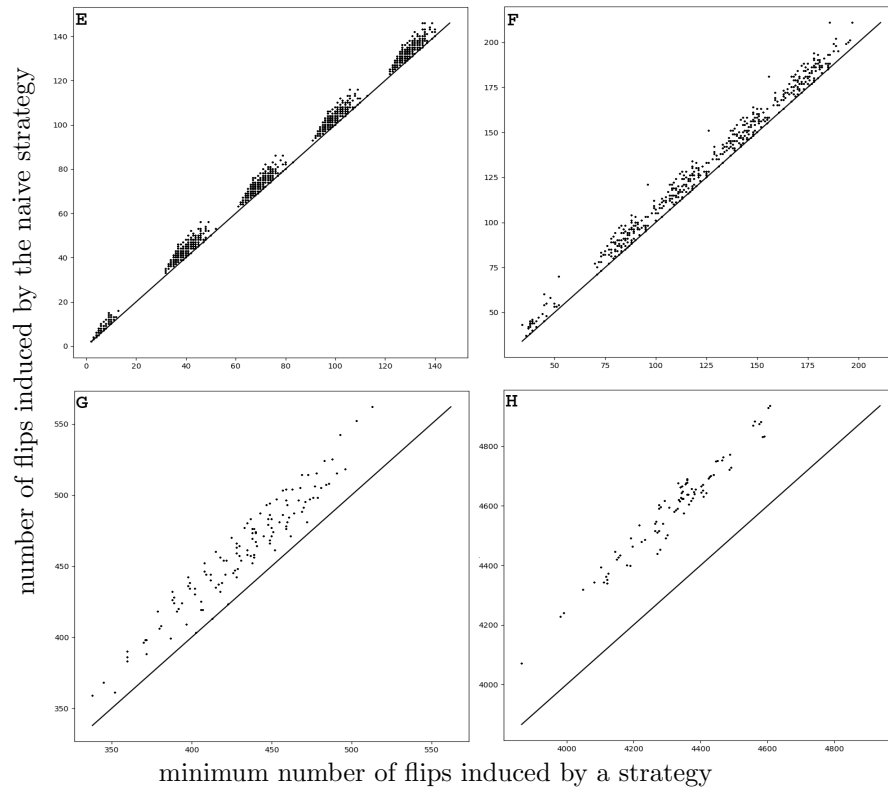


Figure 11: Same as Figure 10, for experiments E, F, G, and H.

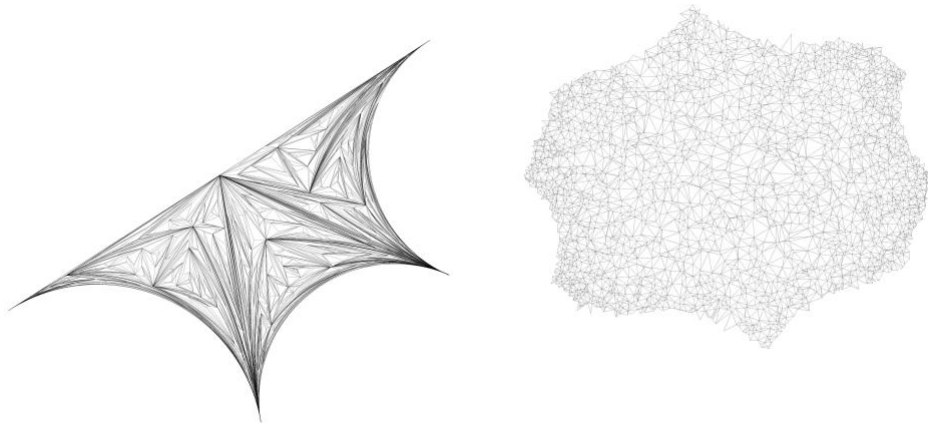


Figure 12: Triangulation with 3001 vertices before (left) and after (right) the flips.

geometric setting), then in the first stage both strategies aim at reducing edge lengths. Thus the two problems might have a similar asymptotic efficiency.

This raises two questions:

- Is there any hope to experimentally observe such similarities in the efficiency? It looks *a priori* unpromising as the above only holds asymptotically.
- Can Mark Bell’s result be transposed to the number of flips?

We carry out two sets of experiments. The first set constructs the input triangulation by twisting the initial octagon in one direction only; as these twists correspond to reducible elements of $\text{Mod}(S_2)$ (Section 2.3) we expect to observe a linear number of flips. The second set of experiments twists the octagon in a random way; asymptotically, we should obtain pseudo-Anosov elements of the mapping class group and an asymptotic logarithmic behavior.

We present five experiments named I, J, K, L, and M, all using the naive strategy (see Section 6). We use again the same notation as in Section 5. We follow steps 3 and 4 and keep track of the loosely-symmetric octagon $G[\mathbf{z}_0', \dots, \mathbf{z}_7']$ obtained in step 4 after the twists; we compute (an approximation represented by a C++ `double` of) the hyperbolic diameter of $G[\mathbf{z}_0', \dots, \mathbf{z}_7']$ (see Appendix E). As we are only interested in the influence of the diameter, we do not run step 2 (i.e., we set $n_p = 0$) and the triangulation thus has only one vertex.

7.2 Exploring with power sequences

Experiments I and J are parameterized by the number n_q of 4-tuples: $n_q = 1$ in I and $n_q = 1,000$ in J. We perform step 4 with $(\mathbf{z}_0, \mathbf{z}_1, \mathbf{z}_2, \mathbf{z}_3) = Q_k$, $n_p = 0$, and $t_1 \dots t_m = u^{3m}$ for $k \in \{1, \dots, n_q\}$, $u \in \{0, 1, 2, 3\}$, and $m \in \{0, \dots, 50\}$, and we compute the approximate hyperbolic diameter $\varnothing_{k,m,u}$ of $G[\mathbf{z}_0', \dots, \mathbf{z}_7']$. We run the Delaunay flip algorithm, counting the number $\alpha_{k,m,u}$ of flips needed for the algorithm to terminate. Figure 13 shows the result.

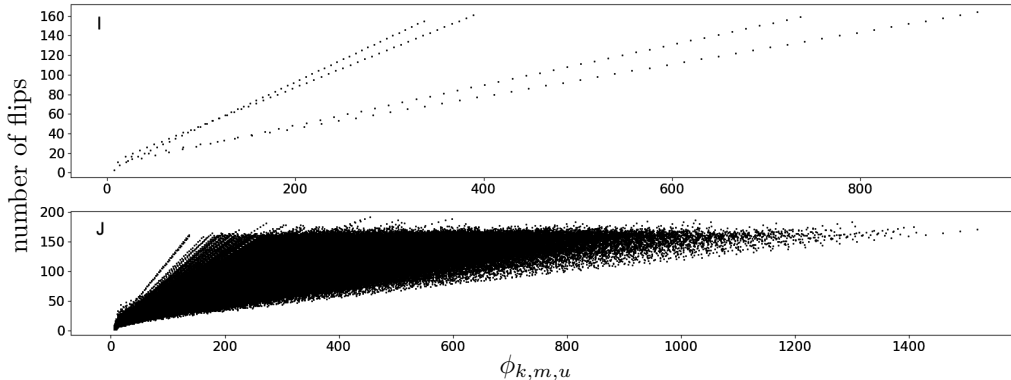


Figure 13: Experiments I and J: the number of flips $\alpha_{k,m,u}$ with respect to the (approximate) diameter $\varnothing_{k,m,u}$, $k \in \{1, \dots, n_q\}$, $m \in \{0, \dots, 50\}$, $u \in \{0, 1, 2, 3\}$.

7.3 Exploring with random sequences

In the following experiments the values of n_q and n_s are respectively $n_q = 1, n_s = 10,000$ (experiment *K*), $n_q = 10, n_s = 1,000$ (experiment *L*), and $n_q = 1,000, n_s = 100$ (experiment *M*). We first construct the set X containing the 11 prefixes of S_l (including the empty sequence) for every $l \in \{1, \dots, n_s\}$. Then for every $k \in \{1, \dots, n_q\}$ and every $t \in X$, we perform step 4 with $(\mathbf{z}_0, \mathbf{z}_1, \mathbf{z}_2, \mathbf{z}_3) = Q_k$, $n_p = 0$, and $t_1 \dots t_m = t$. We compute the approximate diameter $\varnothing_{k,t}$ of $G[\mathbf{z}_0', \dots, \mathbf{z}_7']$. We run the Delaunay flip algorithm and count the number $\alpha_{k,t}$ of flips needed for the algorithm to terminate. Figure 14 shows $\alpha_{k,t}$ as a function of $10 \ln(\varnothing_{k,t})$ for $k \in \{1, \dots, n_q\}$ and $t \in X$. Here \ln denotes the natural logarithm (base e).

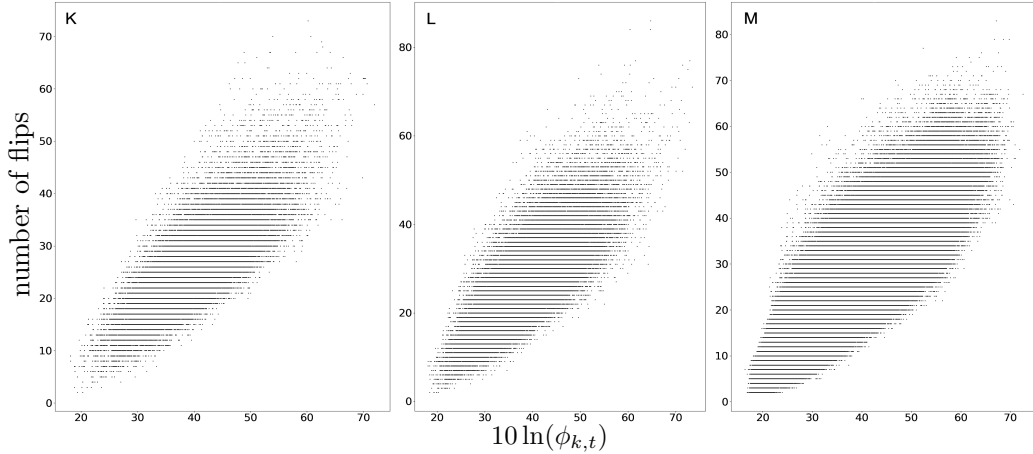


Figure 14: Experiments K, L, and M: the number of flips with respect to $10 \ln(\phi_{k,t})$, $k \in \{1, \dots, n_q\}$, $t \in X$; the maximum diameter is about 1500.

440 **7.4 Interpretation of the results**

441 Our experiments show that controlling the elements of the mapping class group $\text{Mod}(S_2)$ used for
 442 twisting actually allows us to control the number of flips needed by the flip algorithm. Indeed, in
 443 the case of power sequences, we observe that the number of flips is linear in the diameter of the
 444 input triangulation: Delaunay flips untwist the triangulation by performing a constant number
 445 of flips per iteration of the twist. For random sequences, we observe that the number of flips is
 446 logarithmic in the diameter of the input triangulation. In practice the Delaunay flip algorithm
 447 actually realizes a strategy that is as efficient as Mark Bell's.

448 Surprisingly, the asymptotic behavior of random walks in the mapping class group can be
 449 observed in practice with relatively small sequences of twists: even rather short random sequences
 450 reach pseudo-Anosov homeomorphisms, yielding the logarithmic behavior.

451 Some of the experiments use a single input surface while other experiments use up to 1,000
 452 different input surfaces. The behaviors observed do not depend on the surface.

453 In light of our experimental results, we conjecture that the complexity of the Delaunay flip
 454 algorithm is worst-case linear in the diameter of the triangulation, and logarithmic on average.
 455 It should *a priori* not depend on the genus, as Mark Bell's and Maher's results hold for any
 456 genus $g \geq 2$.

References

- 457
- 458 [1] Aline Aigon-Dupuy, Peter Buser, Michel Cibils, Alfred F. Künzle, and Frank Steiner. Hyper-
459 bolic octagons and Teichmüller space in genus 2. *Journal of mathematical physics*,
460 46(3):033513, 2005. doi:10.1063/1.1850177.
- 461 [2] Mark C. Bell. Simplifying triangulations. *Discrete & Computational Geometry*, 66(1):1–11,
462 2021. doi:10.1007/s00454-021-00309-0.
- 463 [3] M. Berger. *Geometry (vols. 1-2)*. Springer-Verlag, 1987.
- 464 [4] Peter Buser. *Geometry and Spectra of Compact Riemann Surfaces*. Birkhäuser, Boston,
465 1992. doi:10.1007/978-0-8176-4992-0.
- 466 [5] Guillaume Damiand. Combinatorial maps. In *CGAL User and Reference Manual*.
467 CGAL Editorial Board, 5.2.1 edition, 2021. URL: [https://doc.cgal.org/5.2.1/Manual/
468 packages.html#PkgCombinatorialMaps](https://doc.cgal.org/5.2.1/Manual/packages.html#PkgCombinatorialMaps).
- 469 [6] Vincent Despré, Benedikt Kolbe, and Monique Teillaud. Representing infinite hyperbolic
470 periodic Delaunay triangulations using finitely many Dirichlet domains. Research report,
471 INRIA, July 2021. URL: <https://hal.inria.fr/hal-03045921>.
- 472 [7] Vincent Despré, Jean-Marc Schlenker, and Monique Teillaud. Flipping geometric trian-
473 gulations on hyperbolic surfaces. In *Proceedings of the 36th International Symposium on
474 Computational Geometry (SoCG'20)*, pages 35:1–35:16, 2020. doi:10.4230/LIPIcs.SoCG.
475 2020.35.
- 476 [8] Matthijs Ebbens, Jordan Iordanov, Monique Teillaud, and Gert Vegter. Delaunay tri-
477 angulations of generalized Bolza surfaces. Research report, INRIA, 2021. URL: [https:
478 //hal.inria.fr/hal-03080125](https://hal.inria.fr/hal-03080125).
- 479 [9] Benson Farb and Dan Margalit. *A primer on mapping class groups*, volume 49 of *Prince-
480 ton Mathematical Series*. Princetown University Press, Princetown, 2012. doi:10.1515/
481 9781400839049.
- 482 [10] Albert Fathi, François Laudenbach, and Valentin Poénaru. *Thurston's Work on Surfaces
483 (MN-48)*. Princeton University Press, 2012.
- 484 [11] Michael Hemmer, Susan Hert, Sylvain Pion, and Stefan Schirra. Number types. In *CGAL
485 User and Reference Manual*. CGAL Editorial Board, 5.3 edition, 2021. URL: [https://doc.
486 cgal.org/5.3/Manual/packages.html#PkgNumberTypes](https://doc.cgal.org/5.3/Manual/packages.html#PkgNumberTypes).
- 487 [12] John H. Hubbard. *Teichmüller Theory and Applications to Geometry, Topology, and Dy-
488 namics*, volume 1. Matrix Editions, 2006.
- 489 [13] Jordan Iordanov and Monique Teillaud. Implementing Delaunay triangulations of the Bolza
490 surface. In *Proceedings of the 33rd International Symposium on Computational Geometry
491 (SoCG'17)*, pages 44:1–44:15, 2017. doi:10.4230/LIPIcs.SoCG.2017.44.
- 492 [14] Nikolai V. Ivanov. *Subgroups of Teichmüller modular groups*, volume 115 of *Translations of
493 Mathematical Monographs*. American Mathematical Soc., 1992. doi:10.1090/mmono/115.
- 494 [15] Joseph Maher. Random walks on the mapping class group. *Duke Mathematical Journal*,
495 156(3):429–468, 2011. doi:10.1215/00127094-2010-216.
- 496 [16] Bojan Mohar and Carsten Thomassen. *Graphs on Surfaces*. Johns Hopkins University Press,
497 Baltimore, 2001.

498 [17] Georg Osang, Mael Rouxel-Labbé, and Monique Teillaud. Generalizing CGAL periodic
 499 Delaunay triangulations. In *Proceedings 28th European Symposium on Algorithms*, pages
 500 75:1–75:17, 2020. Best Paper Award (Track B: Engineering and Applications). doi:10.
 501 4230/LIPIcs.ESA.2020.75.

502 [18] Chee Yap *et al.* The CORE library project. URL: http://cs.nyu.edu/exact/core_pages/.

503 A Cross-ratios and Delaunay flips

504 We define the map $\phi : \mathbb{C} \times \mathbb{C} \rightarrow \mathbb{C}$ by $\phi(x, y) = 1 - (1 - x) \cdot y$ for every $(x, y) \in \mathbb{C}^2$.

505 To prove Lemma 5, we first give a straightforward lemma. Here, the triangulation \mathcal{T} may be
 506 infinite or finite.

507 **Lemma 4.** *Consider a triangulation \mathcal{T} of \mathbb{H} and an edge e of \mathcal{T} . Denote by f, g, h, k the edges,
 508 oriented counter-clockwise, of the quadrilateral formed by the two triangles of \mathcal{T} that are incident
 509 to e (hence assuming that e is incident to two bounded faces). Assume that e is Delaunay-flippable
 510 and let \mathcal{T}^* be the triangulation obtained from \mathcal{T} when replacing e by the other diagonal e^* of the
 511 quadrilateral. Then:*

- 512 • $\mathcal{R}_{\mathcal{T}^*}(e^*) = \mathcal{R}_{\mathcal{T}}(e) / (\mathcal{R}_{\mathcal{T}}(e) - 1)$.
- 513 • $\mathcal{R}_{\mathcal{T}^*}(w) = \phi(\mathcal{R}_{\mathcal{T}}(w), \mathcal{R}_{\mathcal{T}}(e))$ for $w \in \{f, h\}$.
- 514 • $\mathcal{R}_{\mathcal{T}^*}(w) = \phi(\mathcal{R}_{\mathcal{T}}(w), 1/\mathcal{R}_{\mathcal{T}}(e^*))$ for $w \in \{g, k\}$.

515 It is clear that the cross-ratio of any edge of \mathcal{T} other than $\{e, f, g, h, k\}$ remains unchanged
 516 after the flip.

517 *Proof.* Consider the notation defined by Figure 15.

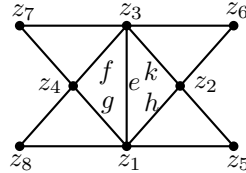


Figure 15: Notation for the proof of Lemma 4 (geodesic edges are represented by straight line segments).

518 A straightforward computation gives:

$$\begin{aligned}
 [z_1, z_2, z_5, z_3] \cdot [z_1, z_2, z_3, z_4] &= [z_1, z_2, z_5, z_4] \\
 [z_2, z_3, z_6, z_4] \cdot [z_2, z_3, z_4, z_1] &= [z_2, z_3, z_6, z_1] \\
 [z_3, z_4, z_7, z_1] \cdot [z_1, z_2, z_3, z_4] &= [z_3, z_4, z_7, z_2] \\
 [z_4, z_1, z_8, z_2] \cdot [z_2, z_3, z_4, z_1] &= [z_4, z_1, z_8, z_3].
 \end{aligned}$$

519 The result follows. □

520 Let us now state the result on \mathcal{S} .

521 **Lemma 5.** *Consider a triangulation T of \mathcal{S} and an edge e of T . Let f, g, h, k be the edges of T
 522 such that e, f, g and e, h, k (oriented counter-clockwise) bound the triangles incident to e in T .
 523 Assume that e is Delaunay-flippable and let T^* be the triangulation obtained from T after the flip
 524 of e and e^* be the new edge replacing e . Then the following holds:*

- 525 • $\mathcal{R}_{T^*}(e^*) = \mathcal{R}_T(e)/(\mathcal{R}_T(e) - 1)$.
- 526 • If $f \neq h$ then $\mathcal{R}_{T^*}(w) = \phi(\mathcal{R}_T(w), \mathcal{R}_T(e))$ for every $w \in \{f, h\}$.
- 527 • If $f = h$ then $\mathcal{R}_{T^*}(f) = \phi(\phi(\mathcal{R}_T(f), \mathcal{R}_T(e)), \mathcal{R}_T(e))$.
- 528 • If $g \neq k$ then $\mathcal{R}_{T^*}(w) = \phi(\mathcal{R}_T(w), 1/\mathcal{R}_{T^*}(e^*))$ for every $w \in \{g, k\}$.
- 529 • If $g = k$ then $\mathcal{R}_{T^*}(g) = \phi(\mathcal{R}_T(g), \phi(\mathcal{R}_T(g), 1/\mathcal{R}_{T^*}(e^*)), 1/\mathcal{R}_{T^*}(e^*))$.

530 Before going to the proof, note that some edges in $X = \{e, f, g, h, k\}$ may be equal. However,
 531 the edges e, f, g are pairwise-distinct and so are the edges e, h, k as they bound faces of \tilde{T} . Also,
 532 $f \neq k$ and $g \neq h$ because the interior angles of the faces of T are all less than π . Hence the only
 533 two possible equalities in X are between f and h , and between g and k .

534 One easily sees that the cross-ratio of any edge $w \notin X$ remains unchanged after the flip.

535 *Proof.* Consider the lift \tilde{T} of T . Choose a fixed lift \tilde{e} of e and let $\tilde{f}, \tilde{g}, \tilde{h}, \tilde{k}$ be the edges of \tilde{T}
 536 such that $\tilde{e}, \tilde{f}, \tilde{g}$ and $\tilde{e}, \tilde{h}, \tilde{k}$ bound the two faces incident to \tilde{e} in \tilde{T} , oriented counter-clockwise.
 537 By renaming \tilde{f}, \tilde{g} to \tilde{h}, \tilde{k} and *vice versa* if needed we can also assume that each $w \in X$ is lifted
 538 by \tilde{w} . We define \tilde{X}_1 as $\{\tilde{f}, \tilde{h}\}$ if $f \neq h$ or as $\{\tilde{f}\}$ if $f = h$. We define \tilde{X}_2 similarly for g and k .
 539 Then we set $\tilde{X} = \{\tilde{e}\} \cup \tilde{X}_1 \cup \tilde{X}_2$. This way \tilde{X} contains exactly one lift of each element of X .
 540 Define \tilde{E} as the set of all lifts of e that are incident to one of the faces of \tilde{T} having an edge in \tilde{X} .
 The possible configurations are summarized in Figure 16. Consider the infinite triangulation \tilde{T}'

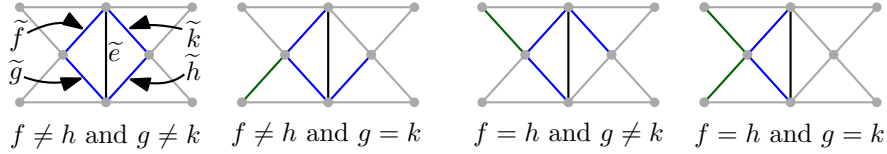


Figure 16: The possible configurations: \tilde{e} is the black segment, $\tilde{X} \setminus \{\tilde{e}\} = \tilde{X}_1 \cup \tilde{X}_2$ is in blue, and $\tilde{E} \setminus \{\tilde{e}\}$ is in green.

541 of the hyperbolic plane obtained from \tilde{T} after flipping each element of \tilde{E} . We denote by \tilde{e}^* the
 542 edge of \tilde{T}' resulting from the flip of \tilde{e} . Then for every $\tilde{w} \in \tilde{X} \setminus \{\tilde{e}\}$ we have $\mathcal{R}_{T^*}(w) = \mathcal{R}_{\tilde{T}'}(\tilde{w})$
 543 and $\mathcal{R}_T(w) = \mathcal{R}_{\tilde{T}}(\tilde{w})$. Also, $\mathcal{R}_{T^*}(e^*) = \mathcal{R}_{\tilde{T}'}(\tilde{e}^*)$ and $\mathcal{R}_T(e) = \mathcal{R}_{\tilde{T}}(\tilde{e})$. The result follows by
 544 computing $\mathcal{R}_{\tilde{T}'}(\tilde{w})$ and $\mathcal{R}_{\tilde{T}'}(\tilde{e}^*)$ using Lemma 5. \square

546 B Details for the representation of triangulations (Section 3)

547 B.1 On combinatorial maps and the anchor (Section 3.1)

548 A 2-dimensional combinatorial map can be described as a finite set whose elements are called
 549 darts together with three permutations β_0, β_1 , and β_2 of this set of darts. The permutations
 550 β_0 and β_1 are the inverse of each other while the permutation β_2 is an involution. We use 2-
 551 dimensional combinatorial maps to describe graphs cellularly embedded on surfaces as follows.
 552 For each face of a graph we constitute a cycle of darts such that given a dart d the next dart
 553 in the cycle is $\beta_1(d)$ (and thus the previous one is $\beta_0(d)$). The darts of the cycle represent the
 554 edges bordering the face. We "glue" faces along their borders by pairing darts: given two darts
 555 d and d' we set $\beta_2(d) = \beta_2(d')$. It is possible to identify two darts that belong to a single face.
 556 We refer to the literature for a formal definition [16, Section 3.3].

557 Now we explain the role played by the anchor A in the data structure (M, F, A) described in
 558 Section 3.1. If z_1, z_2, z_3 , and z_4 denote 4 distinct complex numbers then the number z_4 can be
 559 deduced from z_1, z_2 , and z_3 and from the cross-ratio $[z_1, z_2, z_3, z_4]$. This fact has a consequence
 560 useful to us: given an infinite triangulation \mathcal{T} of the hyperbolic plane if one knows the coordinates

561 in \mathbb{D} of the 3 vertices of some face of \mathcal{T} together with the cross-ratio of every edge of \mathcal{T} then one
 562 can recursively compute the coordinates of any point of \mathcal{T} . In our setting \mathcal{T} is the lift \tilde{T} of a
 563 triangulation T of a surface and for every edge e of T we have $\mathcal{R}_{\tilde{T}}(\tilde{e}) = \mathcal{R}_T(e)$ by definition. In
 564 the data structure (M, F, A) representing the triangulation T the cross-ratios of \tilde{T} are given by
 565 F and the anchor A provides the coordinates of the 3 vertices of some face of \tilde{T} . Consequently
 566 given (M, F, A) one can construct the coordinates of the vertices of \tilde{T} . That enables drawing
 567 some part of \tilde{T} for example (this is our use of the anchor).

568 B.2 Flipping edges (Section 3.2)

569 In this section, we explain how the flip of an edge e of a triangulation T is encoded on the data
 570 structure (M, F, A) defined in Section 3.1 and representing T . We may not make the distinction
 571 between the edges of the triangulation T and those of the combinatorial map M . We are given
 572 as input a dart d_e of the combinatorial map M belonging to the edge e to be flipped. The edge
 573 flip is performed in three steps. Algorithms 1, 2, and 3 are performed in this order. In particular
 574 Algorithms 2 and 3 use the variables d_f, d_g, \dots defined in Algorithm 1. We use the notation of
 575 Section 3.1. We recall here that F denotes the function that maps each edge of the combinatorial
 576 map M to its cross-ratio and $A = (\delta, a_1, a_2, a_3)$ is the anchor.

577 Algorithm 1 performs operations in the combinatorial map M (Figure 17), and is implemented
 578 using the CGAL package [5].

$$\begin{aligned}
 d_f &\leftarrow \beta_1(d_e); \\
 d_g &\leftarrow \beta_1(d_f); \\
 d'_e &\leftarrow \beta_2(d_e); \\
 d_h &\leftarrow \beta_1(d'_e); \\
 d_k &\leftarrow \beta_1(d_h); \\
 \beta_1(d_f), \beta_1(d_e), \beta_1(d_k) &\leftarrow d_e, d_k, d_f; \\
 \beta_1(d_g), \beta_1(d_h), \beta_1(d'_e) &\leftarrow d_h, d'_e, d_g; \\
 \beta_0(d_e), \beta_0(d_k), \beta_0(d_f) &\leftarrow d_f, d_e, d_k; \\
 \beta_0(d_h), \beta_0(d'_e), \beta_0(d_g) &\leftarrow d_g, d_h, d'_e;
 \end{aligned}$$

Algorithm 1: Flipping the edge containing a dart d_e in a combinatorial map.

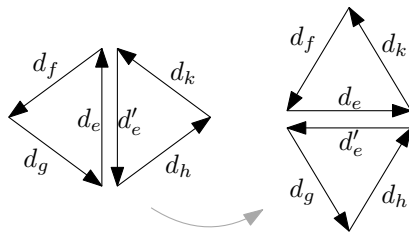


Figure 17: Illustration of Algorithm 1

579 In Algorithms 2 and 3 given a dart d of the combinatorial map M we denote by $[d]$ the edge
 580 that contains d . Algorithm 2 computes an anchor for the triangulation T^* obtained after the flip.
 581 Recall that the lift \tilde{T}^* of T^* is precisely the infinite triangulation of \mathbb{H} obtained by flipping the
 582 lifts of the edge e (there are infinitely many of them) in the lift \tilde{T} of T . Before the flip the anchor
 583 A represents a face \tilde{t} of \tilde{T} . We assume that \tilde{t} is adjacent to a lift \tilde{e} of the edge e to be flipped
 584 (otherwise Algorithm 2 does nothing and the anchor is correctly not modified). Let e^* be the edge
 585 obtained after the flip of e in T and \tilde{e}^* be the lift of e^* obtained after the flip of \tilde{e} in \tilde{T} . We claim
 586 that after the execution of Algorithm 2 the new anchor represents one of the two faces of \tilde{T}^* that
 587 are incident to \tilde{e}^* . First observe that such a face, name it \tilde{t}^* , shares two vertices with \tilde{t} and that
 588 the vertex of \tilde{t}^* that is not shared with \tilde{t} can be computed from the three vertices of \tilde{t} and the

589 cross-ratio of e in T : this computation is done by a function ϕ that we now define. Let $\Omega \subset \mathbb{C}^4$
 590 be the set of 4-tuples $(x, y, z, r) \in \mathbb{C}^4$ such that x, y, z are pairwise-distinct and $r(z - y) \neq (z - x)$.
 591 Then $\phi : \Omega \rightarrow \mathbb{C}$ is defined by $\phi(x, y, z, r) = (xr(z - y) + y(x - z)) / (r(z - y) + x - z)$ on every
 592 $(x, y, z, r) \in \Omega$. The map ϕ is well-defined. Now we briefly explain why ϕ computes this third
 593 vertex of \tilde{t}^* and why Algorithm 2 always gives to ϕ inputs that are in Ω . Consider an infinite
 594 triangulation \mathcal{T} of \mathbb{H} and an edge w of \mathcal{T} . Denote by u_1 and u_3 the vertices of w and by u_2
 595 and u_4 the two other vertices of the two faces of \mathcal{T} containing w : assume that u_1, u_2, u_3, u_4
 596 are in counter-clockwise order. A simple computation shows that $(u_1, u_2, u_3, \mathcal{R}_{\mathcal{T}}(w)) \in \Omega$ and
 597 $u_4 = \phi(u_1, u_2, u_3, \mathcal{R}_{\mathcal{T}}(w))$. The correctness of Algorithm 2 follows by case analysis.

```

switch  $\delta$  do
  case  $d_e$  do
    |  $\delta \leftarrow d_h$ ;
    |  $a_2 \leftarrow \phi(a_2, a_3, a_1, F([d_e]))$ ;
  end
  case  $d'_e$  do
    |  $\delta \leftarrow d_f$ ;
    |  $a_2 \leftarrow \phi(a_2, a_3, a_1, F([d_e]))$ ;
  end
  case  $d_f$  or  $d_h$  do
    |  $a_3 \leftarrow \phi(a_1, a_2, a_3, F([d_e]))$ ;
  end
  case  $d_g$  or  $d_k$  do
    |  $a_3 \leftarrow \phi(a_3, a_1, a_2, F([d_e]))$ ;
  end
end
    
```

Algorithm 2: Updating the anchor $A = (\delta, a_1, a_2, a_3)$. The dart δ is modified if $\delta \in \{d_e, d_f, d_g, d'_e, d_h, d_k\}$.

598 The update of the cross-ratios encoded in the map F is done by Algorithm 3. Algorithm 3
 599 is a straightforward implementation of Lemma 5.

```

 $F([d_f]) \leftarrow 1 - (1 - F([d_f])) \cdot F([d_e])$ ;
if  $\beta_2(d_f) = d_h$  then
  |  $F([d_f]) \leftarrow 1 - (1 - F([d_f])) \cdot F([d_e])$ ;
else
  |  $F([d_h]) \leftarrow 1 - (1 - F(d_h)) \cdot F([d_e])$ ;
end
 $F([d_e]) \leftarrow F([d_e]) / (F([d_e]) - 1)$ ;
 $F([d_g]) \leftarrow 1 - (1 - F([d_g])) / F([d_e])$ ;
if  $\beta_2(d_g) = d_k$  then
  |  $F([d_g]) \leftarrow 1 - (1 - F([d_g])) / F([d_e])$ ;
else
  |  $F([d_k]) \leftarrow 1 - (1 - F([d_k])) / F([d_e])$ ;
end
    
```

Algorithm 3: Updating the cross-ratios.

600 C Details for solving arithmetic issues (Section 4)

601 C.1 Experiment on algebraic numbers (Section 4.1)

602 Algorithm 4 updates the cross-ratios through the sequence of 5 flips described in Section 4.1. It
 603 is a straightforward implementation of Lemma 5.

Input: The cross-ratios R_0, \dots, R_4
for $k = 0, \dots, 4$ **do**
 $R_k \leftarrow R_k / (R_k - 1);$
 if $k \geq 1$ **then**
 $R_{k-1} \leftarrow 1 - (1 - R_{k-1}) / R_k;$
 end
 if $k \leq 3$ **then**
 $R_{k+1} \leftarrow 1 - (1 - R_{k+1}) / R_k;$
 end
end

Algorithm 4: Updating R_0, \dots, R_4 along the sequence of 5 flips.

604 C.2 Approximation algorithm (Section 4.2)

605 This section gives additional details on the construction of the rational admissible 4-tuple shown
 606 in the proof of Theorem 2 in Section 4.2.

607 **Definition 6.** Let $z_0, z_1, z_2, z_3 \in \mathbb{D} \setminus \{0_{\mathbb{C}}\}$ and $\varepsilon > 0$. We say that (z_0, z_1, z_2, z_3) is ε -*valid* if for
 608 any $k \in \{0, 1, 2, 3\}$ and $1 \leq l < m \leq 3$ the following properties are satisfied:

- 609 • $\arg z_0 = 0$
- 610 • $0_{\mathbb{C}} \notin B(z_k, \varepsilon)$
- 611 • $\forall x \in B(z_l, \varepsilon), \forall y \in B(z_m, \varepsilon), 0 < \arg x < \arg y < \pi$.

612 Now let $\mu > 0$. If moreover $|\mathcal{A}(G[-z_0, z_0, z_1, z_2, z_3]) - 2\pi| < \mu$ then we call the tuple (z_0, z_1, z_2, z_3)
 613 (ε, μ) -*admissible*.

614 In what follows we consider some $\varepsilon, \mu > 0$ and a rational (ε, μ) -admissible 4-tuple $(\mathbf{z}_0, \mathbf{z}_1, \mathbf{z}_2, \mathbf{z}_3)$.
 615 Algorithm 5 returns a rational admissible 4-tuple $(\mathbf{z}'_0, \mathbf{z}'_1, \mathbf{z}'_2, \mathbf{z}'_3)$ such that $\mathbf{z}'_k \in B(\mathbf{z}_k, \varepsilon)$ for every
 616 $k \in \{0, 1, 2, 3\}$. We prove the correctness of the algorithm in Proposition 8 under certain assump-
 617 tions on ε, μ , and on the input 4-tuple. Before describing the algorithm we state a preliminary
 618 Lemma.

619 **Lemma 7.** *At least one of the 2 triangles $G[-\mathbf{z}_0, \mathbf{z}_2, \mathbf{z}_3]$ and $G[\mathbf{z}_0, \mathbf{z}_2, \mathbf{z}_1]$ has a hyperbolic area*
 620 *bigger than $\frac{\pi}{2} - \frac{\mu}{2}$.*

621 *Proof.* This is clear since $G[-\mathbf{z}_0, \mathbf{z}_0, \mathbf{z}_2]$ is a triangle so its hyperbolic area is at most π . □

Proposition 8 (Correctness of Algorithm 5). *Assume $\varepsilon \in]0, 1[$ and $\mu \in]0, \pi/6[$. We introduce the following parameter:*

$$R = \max_{0 \leq k \leq 3} d(0_{\mathbb{C}}, \mathbf{z}_k).$$

622 *If the following assumption is satisfied:*

$$\varepsilon > 12\mu e^{6R} \tag{2}$$

623 *then Algorithm 5 is well-defined and correct.*

Input : Reals $\varepsilon, \mu > 0$ and a rational (ε, μ) -admissible 4-tuple $(\mathbf{z}_0, \mathbf{z}_1, \mathbf{z}_2, \mathbf{z}_3)$
Output: A rational admissible 4-tuple $(\mathbf{z}'_0, \mathbf{z}'_1, \mathbf{z}'_2, \mathbf{z}'_3)$ s.t. $\mathbf{z}'_k \in B(\mathbf{z}_k, \varepsilon), \forall k$
if $\mathcal{A}(G[-\mathbf{z}_0, \mathbf{z}_2, \mathbf{z}_3]) > \frac{\pi}{2} - \frac{\mu}{2}$ **then**
 $\mathbf{f} : z \mapsto \frac{z+\mathbf{z}_0}{\mathbf{z}_0 z+1}$;
 $P_0 \leftarrow \text{Im} \left[(1 - \mathbf{f}(\mathbf{z}_0)\overline{\mathbf{f}(\mathbf{z}_1)})(1 - \mathbf{f}(\mathbf{z}_1)\overline{\mathbf{f}(\mathbf{z}_2)}) \right]$;
 $P_1 \leftarrow \text{Im} \left[(1 - \mathbf{f}(\mathbf{z}_0)\overline{\mathbf{f}(\mathbf{z}_1)})(1 - \mathbf{f}(\mathbf{z}_1)\overline{\mathbf{f}(\mathbf{z}_2)})(1 - \mathbf{f}(\mathbf{z}_2)\overline{\mathbf{f}(\mathbf{z}_3)}) \right]$;
 $\lambda \leftarrow P_0/(P_0 - P_1)$;
 $V \leftarrow \lambda \mathbf{f}(\mathbf{z}_3)$;
 return $(\mathbf{z}_0, \mathbf{z}_1, \mathbf{z}_2, \mathbf{f}^{-1}(V))$;
else
 $\mathbf{f} : z \mapsto \frac{z-\mathbf{z}_0}{-\mathbf{z}_0 z+1}$;
 $P_0 \leftarrow \text{Im} \left[(1 - \mathbf{f}(\mathbf{z}_3)\overline{\mathbf{f}(-\mathbf{z}_0)})(1 - \mathbf{f}(\mathbf{z}_2)\overline{\mathbf{f}(\mathbf{z}_3)}) \right]$;
 $P_1 \leftarrow \text{Im} \left[(1 - \mathbf{f}(\mathbf{z}_3)\overline{\mathbf{f}(-\mathbf{z}_0)})(1 - \mathbf{f}(\mathbf{z}_2)\overline{\mathbf{f}(\mathbf{z}_3)})(1 - \mathbf{f}(\mathbf{z}_1)\overline{\mathbf{f}(\mathbf{z}_2)}) \right]$;
 $\lambda \leftarrow P_0/(P_0 - P_1)$;
 $V \leftarrow \lambda \mathbf{f}(\mathbf{z}_1)$;
 return $(\mathbf{z}_0, \mathbf{f}^{-1}(V), \mathbf{z}_2, \mathbf{z}_3)$;
end

Algorithm 5: The approximation algorithm.

624 *Proof.* We only consider the case $\mathcal{A}(G[-\mathbf{z}_0, \mathbf{z}_2, \mathbf{z}_3]) > \frac{\pi}{2} - \frac{\mu}{2}$ as the same arguments hold for
 625 the other case after application of Lemma 7. Using the notations introduced in the algorithm
 626 we bound P_0 and P_1 and then deduce that λ is well-defined. Only then we prove that $V \in$
 627 $B(\mathbf{f}(\mathbf{z}_3), \varepsilon)$. We have $P_0 = \text{Im}[Z_0]$ and $P_1 = \text{Im}[Z_1]$ with

$$\begin{aligned}
 Z_0 &= (1 - \mathbf{f}(\mathbf{z}_0)\overline{\mathbf{f}(\mathbf{z}_1)})(1 - \mathbf{f}(\mathbf{z}_1)\overline{\mathbf{f}(\mathbf{z}_2)}) \\
 Z_1 &= (1 - \mathbf{f}(\mathbf{z}_0)\overline{\mathbf{f}(\mathbf{z}_1)})(1 - \mathbf{f}(\mathbf{z}_1)\overline{\mathbf{f}(\mathbf{z}_2)})(1 - \mathbf{f}(\mathbf{z}_2)\overline{\mathbf{f}(\mathbf{z}_3)}).
 \end{aligned}$$

628 We already proved that $\arg Z_1 = \frac{1}{2}\mathcal{A}(G[-\mathbf{z}_0, \mathbf{z}_0, \mathbf{z}_1, \mathbf{z}_2, \mathbf{z}_3])$. Also we have $|\arg Z_1 - \pi| < \frac{\mu}{2}$ since
 629 $(\mathbf{z}_0, \mathbf{z}_1, \mathbf{z}_2, \mathbf{z}_3)$ is (ε, μ) -admissible. Since $\mu < \pi$, $|P_1| < \sin(\frac{\mu}{2}) < \frac{\mu}{2}$. In addition,

$$\begin{aligned}
 \arg Z_0 &= \frac{1}{2}\mathcal{A}(G[-\mathbf{z}_0, \mathbf{z}_0, \mathbf{z}_1, \mathbf{z}_2]) \\
 &= \frac{1}{2}(\mathcal{A}(G[-\mathbf{z}_0, \mathbf{z}_0, \mathbf{z}_1, \mathbf{z}_2, \mathbf{z}_3]) - \mathcal{A}(G[-\mathbf{z}_0, \mathbf{z}_2, \mathbf{z}_3])).
 \end{aligned}$$

By Definition 6, and since $\frac{\pi}{2} - \frac{\mu}{2} < \mathcal{A}(G[-\mathbf{z}_0, \mathbf{z}_2, \mathbf{z}_3]) < \pi$,

$$\frac{\pi}{2} - \frac{\mu}{2} < \arg Z_0 < \frac{3\pi}{4} + \frac{3\mu}{4}.$$

630 Moreover for every $k \in \{0, 1, 2, 3\}$ one has $d(0_{\mathbb{C}}, \mathbf{f}(\mathbf{z}_k)) \leq d(0_{\mathbb{C}}, \mathbf{f}(0_{\mathbb{C}})) + d(\mathbf{f}(0_{\mathbb{C}}), \mathbf{f}(\mathbf{z}_k)) =$
 631 $d(0_{\mathbb{C}}, \mathbf{z}_0) + d(0_{\mathbb{C}}, \mathbf{z}_k) \leq 2R$. Writing the Euclidean norm in term of the hyperbolic distance
 632 d (in the Poincaré disk model) the latter becomes $|\mathbf{f}(\mathbf{z}_k)| \leq \tanh(R)$. That proves $1 \geq |Z_0| \geq$
 633 $(1 - \tanh(R))^2$. Together with the bound on $\arg Z_0$ we obtain a bound on P_0 :

$$\begin{aligned}
 1 > P_0 &> (1 - \tanh(R))^2 \cdot \sin\left(\frac{3\pi}{4} + \frac{3\mu}{4}\right) \\
 &\geq e^{-4R} \cdot \sin\left(\frac{3\pi}{4} + \frac{3\mu}{4}\right) \\
 &> \frac{1}{3}e^{-4R},
 \end{aligned}$$

since $\mu < \frac{\pi}{6}$ and $\sin(\frac{7\pi}{8}) > \frac{1}{3}$. From the bounds on P_0 and P_1 , and using Assumption (2) we deduce that $P_0 > P_1$, so λ is well defined. Also, we get that

$$1 < \lambda < \frac{1}{1 - \frac{3}{2}\mu e^{4R}}.$$

It remains to prove that $V \in B(\mathbf{f}(\mathbf{z}_3), \varepsilon)$. For the sake of clarity we denote by D the hyperbolic distance $d(0_{\mathbb{C}}, \mathbf{f}(\mathbf{z}_3))$. It is enough to show the following:

$$\lambda \tanh\left(\frac{D}{2}\right) < \tanh\left(\frac{D + \varepsilon}{2}\right).$$

We first observe that $x \mapsto \tanh(x) - x/2$ is increasing on $[0, 1/2[$ and maps 0 to 0. Thus, since $\varepsilon/2 \in]0, 1/2[$, $\tanh(\varepsilon/2) \geq \varepsilon/4$. From that and by applying Assumption (2) we obtain

$$\mu e^{4R} < \tanh(\varepsilon/2)e^{-2R}.$$

634 We conclude with the following implications:

$$\begin{aligned} & 3\mu e^{4R} < \tanh(\varepsilon/2)e^{-2R} \\ \implies & \frac{3}{2}\mu e^{4R} < \frac{1}{2}\tanh(\varepsilon/2)(1 - \tanh(R)^2) \\ \implies & \frac{\tanh(D/2) + \tanh(D/2)^2 \tanh(\varepsilon/2)}{\tanh(D/2) + \tanh(\varepsilon/2)} < 1 - \frac{3}{2}\mu e^{4R} \\ \implies & \frac{\tanh(\frac{D}{2})}{\tanh(\frac{D+\varepsilon}{2})} < 1 - \frac{3}{2}\mu e^{4R} \\ \implies & \lambda \tanh\left(\frac{D}{2}\right) < \tanh\left(\frac{D + \varepsilon}{2}\right). \end{aligned}$$

635 That concludes the proof. □

636 D Details for the generation of input (Section 5)

637 D.1 Generating an initial rational 4-tuple (step 1)

638 We follow the construction of 4-tuples [1, Section 3] recalled in Section 2.4 but only compute
 639 rational approximations of the algebraic numbers involved. Then we apply Algorithm 5. The
 640 generation process described below has the following advantage: the size of the integers involved
 641 in the output 4-tuple $(\mathbf{z}_0, \mathbf{z}_1, \mathbf{z}_2, \mathbf{z}_3)$ are controlled by the parameter \mathbb{N} defined below. Providing
 642 small fractions is important as the process described in this section is performed at the very
 643 beginning of the experiments.

644 We first construct for $k \in \{1, 2, 3\}$ the real and imaginary parts x_k and y_k of a complex
 645 number z_k ; they are represented as `float` numbers in python and constructed in $[-1, 1]$ using
 646 the `random` method of the `random` package: $x_k = 2 * \text{random.random()} - 1$. That simulates a
 647 uniform distribution. The construction fails if one of the points $\{z_1, z_2, z_3\}$ lies outside \mathbb{D} , or if
 648 the condition $a + b + c < 0$ with a, b , and c as defined in Section 2.4 is not satisfied.

649 Then we construct the `float` numbers x_0 and y_0 representing the real and imaginary parts
 650 of z_0 as described in Section 2.4. From that we construct for each $k \in \{0, 1, 2, 3\}$ the real
 651 and imaginary parts \mathbf{x}_k and \mathbf{y}_k of \mathbf{z}_k as rational approximations of x_k and y_k : we set $\mathbf{x}_k =$
 652 `int(N * x_k) / N`, where the parameter $\mathbb{N} \in \mathbb{N} \setminus \{0_{\mathbb{N}}\}$ determines the quality of the approximation
 653 and `int` is native in python. We arbitrarily chose $\mathbb{N} = 100$ in each computation. The construction
 654 fails if $(\mathbf{z}_0, \mathbf{z}_1, \mathbf{z}_2, \mathbf{z}_3)$ is not valid.

655 The rational 4-tuple $(\mathbf{z}_0, \mathbf{z}_1, \mathbf{z}_2, \mathbf{z}_3)$ is not necessarily admissible. However, by the construc-
 656 tion method, it can be seen as a rational approximation of some admissible 4-tuple and it satisfies

657 the hypothesis of Proposition 8. We can thus compute an admissible 4-tuple using Algorithm 5
 658 (see also Section 4.2).

659 To simplify notation, we still denote the rational admissible 4-tuple that we obtain by
 660 $(\mathbf{z}_0, \mathbf{z}_1, \mathbf{z}_2, \mathbf{z}_3)$.

661 D.2 Generating points in an admissible symmetric octagon (step 2)

662 Consider the rational admissible 4-tuple $(\mathbf{z}_0, \mathbf{z}_1, \mathbf{z}_2, \mathbf{z}_3)$ obtained after step 1. In this section, we
 663 describe our method to construct a point $\mathbf{p} \in \mathbb{Q} + i\mathbb{Q}$ in the closure of the admissible symmetric
 664 octagon $\mathcal{P}[\mathbf{z}_0, \mathbf{z}_1, \mathbf{z}_2, \mathbf{z}_3]$, simulating a uniform distribution with respect to the hyperbolic metric.

665 The method uses inexact computation so it can fail especially if the Euclidean area of
 666 $\mathcal{P}[\mathbf{z}_0, \mathbf{z}_1, \mathbf{z}_2, \mathbf{z}_3]$ is close to 0. This is also why we do not generate such points in the admis-
 667 sible loosely-symmetric octagons resulting from the twists in step 4.

668 We start by dividing $\mathcal{P}[\mathbf{z}_0, \mathbf{z}_1, \mathbf{z}_2, \mathbf{z}_3]$ into 6 hyperbolic triangles $\Delta_1, \dots, \Delta_6$. We compute the
 669 hyperbolic area of each triangle as a C++ (native) `double` number using Equality (1). Then

670 we choose the triangle Δ_k that will contain \mathbf{p} with probability $\frac{\mathcal{A}(\Delta_k)}{\sum_{l=1}^6 \mathcal{A}(\Delta_l)}$, $k \in \{1, \dots, 6\}$. By

671 a translation we can assume that $0_{\mathbb{C}}$ is a vertex of Δ_k . We construct as `double` numbers the
 672 real and imaginary parts of a complex number $p \in \mathbb{D}$, simulating a uniform choice within the
 673 closure of Δ_k . To construct \mathbf{p} from p we cast the real and imaginary parts of p into `CGAL::Gmpq`
 674 numbers [11]. Then we check using Lemma 9 whether \mathbf{p} actually belongs to the closure of Δ_k ; if
 675 this is the case we return \mathbf{p} .

Lemma 9. *Consider pairwise-distinct points $z_1, z_2, z_3 \in \mathbb{D}$ and the oriented geodesic l containing z_1 and z_2 , oriented from z_1 to z_2 . The oriented geodesic l separates \mathbb{D} into 2 open regions and we consider the region R on the left of l . We define $\tau : \mathbb{D} \rightarrow \mathbb{D}$ by*

$$\tau(z) = \frac{z - z_1}{1 - \bar{z}_1 z}$$

for every $z \in \mathbb{D}$. Then $z_3 \in R$ if and only if

$$\operatorname{Im} \left[\frac{\tau(z_3)}{\tau(z_2)} \right] > 0$$

676 and the above expression is an equality if and only if $z_3 \in l$.

677 *Proof.* The result follows from observing that τ is an orientation preserving isometry of \mathbb{D} sending
 678 z_1 to $0_{\mathbb{C}}$. □

679 D.3 Constructing the data structure (step 4)

680 After step 1, step 2, and step 3, we are given a rational admissible 4-tuple $(\mathbf{z}_0, \mathbf{z}_1, \mathbf{z}_2, \mathbf{z}_3)$, points
 681 $(\mathbf{p}_1, \dots, \mathbf{p}_{n_p}) \in (\mathbb{Q} + i\mathbb{Q})^{n_p}$ lying in the closure of $\mathcal{P}[\mathbf{z}_0, \mathbf{z}_1, \mathbf{z}_2, \mathbf{z}_3]$ and a sequence t_1, \dots, t_m of
 682 twists. The rational admissible 4-tuple $(\mathbf{z}_0, \mathbf{z}_1, \mathbf{z}_2, \mathbf{z}_3)$ defines the surface \mathcal{S} .

683 Applying the procedure in Section 5.1 we construct the vertices $\mathbf{z}_0', \dots, \mathbf{z}_7'$ of the rational
 684 admissible loosely-symmetric octagon resulting from twisting $\mathcal{P}[\mathbf{z}_0, \mathbf{z}_1, \mathbf{z}_2, \mathbf{z}_3]$ according to the
 685 sequence t_1, \dots, t_m . From $\mathbf{p}_1, \dots, \mathbf{p}_{n_p}$ we also construct new points $(\mathbf{p}_1', \dots, \mathbf{p}_{n_p}') \in (\mathbb{Q} + i\mathbb{Q})^{n_p}$
 686 lying in the closure of $G[\mathbf{z}_0', \dots, \mathbf{z}_7']$. The latter is done twist by twist : when performing a twist
 687 on an octagon O we obtain a new octagon O' and we update the list of points so that they lie in
 688 the closure of the octagon O' after the twist. When a point p is replaced by a new point p' we
 689 make sure that p and p' are two lifts of the *same* point on the surface represented by O and O' .
 690 In the end we also compute the orientation preserving isometries $(\tau'_k)_{0 \leq k \leq 7}$ pairing the opposite
 691 sides of $G[\mathbf{z}_0', \dots, \mathbf{z}_7']$ (see Section 5.1).

692 Recursively, we construct a sequence T_0, \dots, T_{n_p} of triangulations of the octagon $G[\mathbf{z}_0', \dots, \mathbf{z}_7']$.
 693 We start with the triangulation T_0 whose edges are the eight sides of $G[\mathbf{z}_0', \dots, \mathbf{z}_7']$, and the
 694 five geodesic segments between \mathbf{z}_0' and $\mathbf{z}_2', \mathbf{z}_3', \mathbf{z}_4', \mathbf{z}_5', \mathbf{z}_6'$. The triangulation T_0 is represented
 695 by a combinatorial map M_0 and a map P_0 associating to each vertex v of M_0 its position $P_0(v)$
 696 in \mathbb{D} . For $k \in \{1, \dots, n_p\}$ the triangulation T_k is obtained from T_{k-1} by splitting the triangle
 697 containing \mathbf{p}_k' into three triangles. In the end we get a triangulation T_{n_p} together with its com-
 698 binatorial map M_{n_p} and the map P_{n_p} giving the position of each vertex in \mathbb{D} . By identifying the
 699 edges of T_{n_p} that are the opposite sides of $G[z'_0, \dots, z'_7]$ we obtain a triangulation T of \mathcal{S} .

700 We finally construct the triple (M, F, A) representing the triangulation T from the com-
 701 binatorial map M_{n_p} and the map P_{n_p} (see Section 3.1). The combinatorial map M is easily
 702 obtained from M_{n_p} by setting $\beta_2(d) = d'$ and $\beta_2(d') = d$ (see Figure 2) for any 2 distinct darts
 703 d and d' of M_{n_p} supporting 2 edges corresponding to opposite sides of $G[z'_0, \dots, z'_7]$. The anchor
 704 $A = (\delta, a_1, a_2, a_3)$ is defined by choosing δ in M_{n_p} : the dart δ belongs to a face (v_1, v_2, v_3) of
 705 M_{n_p} and is based at v_1 ; we set $a_k = P_{n_p}(v_k)$ for every $k \in \{1, 2, 3\}$. Now consider some edge e
 706 of M . There are 2 cases. If e results from an edge of M_{n_p} that was not a side of $G[\mathbf{z}_0', \dots, \mathbf{z}_7']$
 707 then computing its cross-ratio in T_{n_p} or equivalently in T is straightforward. If e results from
 708 the identification of 2 edges e_1 and e_2 of M_{n_p} then we compute $F(e)$ as follows. We denote the
 709 vertices of e_1 in M_{n_p} by a, b and the vertices of e_2 by c, d such that $P_{n_p}(a), P_{n_p}(b), P_{n_p}(c), P_{n_p}(d)$
 710 appear in counter-clockwise order on the boundary of $G[\mathbf{z}_0', \dots, \mathbf{z}_7']$: when identifying e_1 and
 711 e_2 to construct M from M_{n_p} the vertex a is identified with d , and the vertex b is identified
 712 with c . We consider $k \in \{0, \dots, 7\}$ such that orientation preserving isometry τ'_k maps $P_{n_p}(d)$
 713 to $P_{n_p}(a)$ and maps $P_{n_p}(c)$ to $P_{n_p}(b)$. The edge e_1 belongs to a unique face f_1 of M_{n_p} and
 714 we denote the vertex of f_1 that is neither a nor b by u_1 . Similarly, the edge e_2 belongs to a
 715 unique face f_2 of M_{n_p} and we denote the vertex of f_2 that is neither c nor d by u_2 . Then
 716 $F(e) = [P_{n_p}(a), \tau'_k(P_{n_p}(u_2)), P_{n_p}(b), P_{n_p}(u_1)]$.

717 E Computation of the approximation of the diameter (Section 7)

718 Consider a rational admissible loosely-symmetric octagon O given by the 16 rational numbers
 719 representing the real and imaginary parts of its 8 vertices. The hyperbolic diameter of O is the
 720 maximum of the hyperbolic distances between any two of its vertices. For every pair z_1, z_2 of
 721 two such distinct vertices we compute an approximation represented by a C++ `double` D of the
 722 hyperbolic distance between z_1 and z_2 . The maximum (obtained using `std::max`) of these $\binom{8}{2}$
 723 values is an approximation of the hyperbolic diameter of O .

724 We compute every such D as follows. The isometry $f : z \mapsto (z - z_1)/(1 - z_1 z)$ maps $\mathbb{Q} \cap \mathbb{D}$
 725 to a subset of \mathbb{Q} and maps z_1 to 0. We compute the exact rational value r_2 of the square of the
 726 modulus of $f(z_2)$. Then we convert r_2 to a `CORE::Expr` r'_2 and set $x = (1 + \text{CGAL}::\text{sqrt}(r'_2))/(1 -$
 727 $\text{CGAL}::\text{sqrt}(r'_2))$. The number D is an approximation of the natural logarithm $\ln(x)$ of x ob-
 728 tained by first casting x to a string s . The string s contains the string representation s_1 of
 729 the lower integer rounding k of $\log_{10}(x)$. Also s contains the string representation s_2 of an
 730 approximation of $x \cdot 10^{-k}$. The value of D is calculated as `std::stoi(s_1) * std::log(10) +`
 731 `std::log(std::stod(s_2))`.